Different Brain States are Differentially Responsive to Ultrasonic Stimulation

Devon Griggs

A thesis

submitted in partial fulfillment of the

requirements of the degree of

Master of Science in Electrical Engineering

University of Washington

2018

Committee:

Pierre D. Mourad

Tadesse Ghirmai

Hung Cao

Program Authorized to Offer Degree:

Electrical Engineering

University of Washington

Abstract

Different Brain States are Differentially Responsive to Ultrasonic Stimulation

Devon Griggs

Chair of Supervisory Committee:
Pierre Mourad
Division of Engineering & Mathematics

It is well known that direct, non-invasive, spatially specific ultrasonic stimulation of the brain can activate neural responses, however it is less studied how the brain's state itself affects the responses. This thesis explores the differential responses to different brain states in mice, particularly the anesthetized brain state as induced by isoflurane and the sedated, awake-like brain state as induced by medetomidine. The electrocorticographic (ECoG) technique was utilized to record responses in the visual cortex (V1), the somatosensory cortex, and the auditory cortex when a flash of light was cast on the retina of the eye and when a burst of pulsed ultrasound was focused on V1. It was found that the responses due to these two stimulation techniques of the same brain state were largely similar. For example, under isoflurane, each stimulation generated slow waves; under medetomidine, they did not. This preliminary result serves to confirm the effects of different brain states regardless of stimulation technique. Differences were discovered, too. For example, it was also found that direct visual stimulation generated stronger neural responses than did ultrasonic stimulation for both brain states. All results presented here are preliminary due to the small sample size but will guide future studies. Taken together, these preliminary results pave the way to further investigation of the similarities and differences of direct ultrasonic stimulation of the cortex and indirect neural stimulation of the cortex via light cast on the retina of the eye, as well as other sensory input such as sound and pinching, when applied to mice experiencing various brain states.

INTRODUCTION

Ultrasound is a relatively little studied medium by which to modulate brain function and, as the title of the thesis suggests, the brain's response to ultrasonic modulation is itself modulated by the state of the brain. This thesis explores ultrasonic stimulation of two mouse brain states: immediate neural responses of healthy brains under isoflurane anesthesia, and immediate neural responses of healthy brains under medetomidine sedative. To begin, some of ultrasound's properties and applications are described in overview and some relevant data analysis techniques are discussed.

ULTRASOUND AND ITS PHYSICAL PROPERTIES

Ultrasound comes with a set of terminology and calculations, some of which are briefly introduced here.

SOUND, ULTRASOUND, AND TRANSDUCERS

Sound, as we interact with it every day, is variations in air pressure which the mechanical and fluidic components of our ear sense and transduce into electrical impulses which our nerves then carry into the brain to be processed. Human ears have a rather finite hearing frequency range, however, and sounds above the upper bound of that range, which is around 20 kHz, are defined as ultrasounds. In order to force a substance (air or otherwise) to vibrate fast enough to produce ultrasound, makers of ultrasonic transducers typically employ piezoelectric materials which, by definition, may be compressed and expanded by the application of voltage. While what we typically think of as sound is usually not just one frequency of sound but rather multiple frequencies summed together, man-made ultrasound is usually designed, albeit imperfectly, to be emitted at a single frequency.

ULTRASOUND CLASSIFICATIONS

Ultrasound may be classified in various ways, one of them being continuous ultrasound and another being pulsed ultrasound. Where continuous ultrasound is, at its name suggests, a single frequency of ultrasound emitted continuously from a transducer, pulsed ultrasound may be thought of as a continuous ultrasonic signal which is turned off and on, and that typically at regular intervals. In these cases, convention calls the frequency of the ultrasound the carrier frequency and the frequency of the pulses the pulse repetition frequency. Additional classification of ultrasound which may be applied to either continuous or pulsed ultrasound include parameters such as amplitude, pulse duration, and various methods of calculating intensity.

ULTRASOUND INTENSITY

In light of the many different ways to approach ultrasonic application, the calculation of ultrasonic intensity, which is defined as unit power per unit area, also may be accomplished in a variety of ways. The two key parameters influencing the intensity calculation process are the spatial component and temporal component. When a beam of ultrasound is considered spatially, the pressure waves along the direction of the ultrasound orientation will be greater that the pressure waves to the sides. With this in mind, the spatial component may be approached by two methods: The spatial peak intensity may be measured which expresses the maximum effect of the ultrasound, or the spatial average intensity may be measured which is the average of multiple points across the span of the beam. Naturally, the spatial

peak intensity is higher than the spatial average intensity. When a beam of ultrasound is considered temporally with a pulse repetition frequency, three approaches may be taken: The temporal peak intensity may be recorded, a pulse average intensity may be recorded (being the average intensity of a pulse), or a temporal average intensity of all pulses may be recorded including the dead time between pulses due to the pulse repetition frequency. Thus, when all combinations of spatial and temporal components are considered, six different calculations of intensity arise. Of these, the FDA (Food and Drug Administration) provide guidelines for spatial peak temporal average intensity (I_{spta}), which is most relevant to this thesis.

ULTRASONIC NEURAL STIMULATION

Here theories of the mechanism which allows ultrasound to stimulate neurons is briefly discussed, followed by an introduction to the techniques of stimulation and the choices of anesthesia or sedatives to enable stimulation, the constituent effects of stimulation, and finally a brief scrutiny of electrophysiological recording.

THEORY

The exact process by which ultrasound stimulates neurons is, unfortunately, still unclear, yet is a process keenly studied (Rezayat E 2016). One hypothesis is that the application of ultrasound on a neuron can activate voltage-gated calcium and sodium channels and thus trigger the neuron to fire (Tyler WJ 2008) and other theories suggest that the radiative force (i.e., the phenomenon of pushing objects with which the acoustic waves interact) affects membrane capacitance (Plaksin M 2014) or nitric oxide synthesis (Sugita Yoichi 2008). Although cliché, more research is needed.

TECHNIQUES

Concerning the medical realm, ultrasound is perhaps best known for its utility in fetal imaging and other imagining tasks. In this thesis research is discussed on less pervasive utilities of ultrasound, being demonstrated ability of ultrasound (often of the pulsed and focused variety (Tufail Y 2010, Bystritsky A 2011)) to stimulate, and in some cases provide therapy to (Bauer R 2014, Lipsman N 2013), the brain. Ultrasound has a unique place in the realm of neural stimulation because of its non-invasiveness and its spatial specificity. Where techniques such as optogenetics and neural implants have the benefits of high special specificity, they require invasive surgical procedures. Meanwhile, techniques such as magnetic stimulation and some forms of electrical stimulation are non-invasive but they suffer from a lack of spatial specificity (although at least one research group claims to have non-invasively solved the electrical neural stimulation spatial specificity problem (Grossman N 2017), and that using a technique analogous to a technique previously used by the ultrasonic neural stimulation community (Mehić E 2014), this electrical neural stimulation technique has not yet come to be accepted at large). Ultrasound, at least for the current techniques of neural activation and therapy, is often completely non-invasive. There are techniques which involve the injection of acoustic agents into the circulatory system which may be used for cranial ultrasonic applications (Errico C 2015) and in the future “neural dust” (Seo D 2016), which are tiny ultrasonically powered electronic devices (and which would arguably not be considered a true ultrasonic neural stimulation technique), may be implanted in the brain, but the transducer hardware need not break skin regardless. Ultrasonic devices rely on acoustically clear (and,

coincidently, typically optically clear) gel situated between the device and the skin which allows the ultrasound to pass from the device into body with relatively little energy loss due to reflection at the interfaces of the mediums. Ultrasound's spatial specificity is a direct use of the phenomenon where pressure waves which collide may sum constructively to produce greater effect. One or more carefully designed and aimed (by hand or otherwise) piezoelectric crystals, sometimes aided with carefully timed-staggered electric activation, can create an ultrasonic focus at a desired point in the three-dimensional space of the brain. While implementation accuracy, predetermined ultrasonic parameters, and pressure thresholds for what spatial region extent is considered the focus of the ultrasound cause the size of that focus to vary, this focus can generally be thought of as roughly the size of a grain of rice.

ANESTHESIA AND SEDATIVES

In order to be studied, the mice were put under anesthesia or a sedative. In the study of visual and ultrasonic stimulation of healthy mice, isoflurane and medetomidine were chosen. Isoflurane, a type of anesthesia, puts mice in non-REM sleep brain states. Medetomidine, a type of sedative, keeps the mouse in an awake brain state yet relieves the mouse of anxiety and discomfort arising from the experimental procedure. These drugs allow for study of the mice under different brain states. Isoflurane in particular was selected as the anesthesia because it may be inhaled. This allows the anesthesia to be adjusted or turned off rather quickly as desired. Furthermore, since the effects of isoflurane tails off rather quickly after the mouse stops inhaling it, the same mouse, after initially sedated via medetomidine injection, could be alternated from an awake brain state to a non-REM sleep brain state and vice-verses in an acceptable amount of time based on the application of isoflurane.

EFFECTS

The study of the effects of ultrasonic neural stimulation usually fall into one of the following categories: behavioral, histological, and electrophysiological. Behavioral observations may be used to study the effects of ultrasound post-application on such things as improving memory retention (Lin WT 2015), impairment of learning (Miller DL 1991), levels of activity (McClintic AM 2014),and autism spectrum disorder symptoms (Webb SJ 2017), and the real time effects of ultrasound such as the evocation of motor movement (Mehić E 2014). Histological observations may be used to study evoked physiological changes such as disruption to the blood-brain-barrier (Mesiwala AH 2002) or remyelination of previously demyelinated neurons (Olmstead TA 2018). Electrophysiological observations also come in a variety of techniques and with an array of goals. Electrophysiological observation techniques include electroencephalography (EEG), where a non-invasive electrode is situated on the scalp, electrocorticography (ECoG), where a moderately invasive electrode is placed on the surface of the brain, and implants, where a highly-invasive electrode is implanted into the brain tissue. A schematic of a mouse brain is shown in Figure 1. Depending on the variation of techniques employed, and the variation in large part being the amount of conductor allowed to make contact with the neural tissue, the signal read from the electrodes may represent global brain activity, local brain activity, or even activity of individual neurons, which itself is a technique known as patch clamp. Because this study is focused on the activity in regions of the brain, specifically the auditory cortex (A1), the somatosensory cortex (S1), and the visual cortex (V1), using electrodes to read local brain activity was the natural choice. A schematic of the mouse brain is shown in Figure 1. Reading the signals from A1 poses a unique concern in that ultrasound directed into the mouse's head may cause movement of the mechanical and

fluidic structures in the ear and thus trigger the brain to respond as if it were audibly stimulated. This potential phenomenon may be explored in the future with experimentation on deaf mice in an effort to eliminate any opportunity for ultrasound to drive spurious responses in A1.

ELECTROPHYSIOLOGICAL RECORDING CONSIDERATIONS

Electrophysiological recording has its drawbacks. In addition to recording the electrical signals supplied by the brain, the electrodes and associated wires are liable to pick up noise, and these noises may come from a variety of sources such as heartbeat, motor movements of the mouse, noise from other electronics, and even noise from crosstalk with other wires. To mitigate several of these challenges, temporal averages (discussed below) were taken to smooth out their effects. To further mitigate the challenges of noise derived from motor movements, the mice were either sedated or anesthetized to reduce motor movement. To mitigate challenges of noise from other electronics, mice were generally situated in the laboratory away from noisy electronics. The wire crosstalk challenges were mitigated with electrode wires manufactured to optimize recording of the local cortical area and generally positioned to reduce crosstalk between wires. Crosstalk occurs when electric and magnetic fields interact in theoretically understood phenomena such as inductive coupling, capacitive coupling, and direct coupling, but although these are theoretically understood these effects can be difficult to manage in practice. Because the mouse brain areas studied (being the visual cortex, the auditory cortex, and the somatosensory cortex) for this thesis are close together the wires and electrodes must come in close proximity, thus amplifying the opportunity for crosstalk noise.

DATA ANALYSIS TECHNIQUES

Electrophysiological recording means little without proper data analysis techniques and a sufficient understanding of the associated terminology. Selected topics are discussed below.

DATA STRUCTURE

After the electrodes where situated in different regions on the brain, data was recorded from these electrodes, called channels. Data recording the activity of equipment such as LEDs and ultrasonic transducers are recorded in separate channels, as well. Example data are shown in Figure 2 where different colors represent the data from different brain areas and the purple arrows indicate the time of stimulation. Example data are shown in Figure 2 across a smaller window of time where close inspection may reveal details such as visually stimulated neural activation and heartbeat as indicated by yellow and red arrows, respectively, in addition to the distinct channels of the different brain regions and the channel of stimulation. Segments of this data from 4.5 seconds before to 4.5 seconds after the onset of stimulation were extracted and are called “events”. For analysis purposes in calculations yet to be described, 3.8-0.2 seconds before the stimulation onset shall be referred to as “background”, 0-0.2 seconds after the onset shall be referred to as the “spike”, and 0.2-3.0 seconds after the stimulation onset shall be referred to as the “residual”. These choices are depicted in Figure 4.

TEMPORAL AVERAGES

Temporal averages were used to minimize activity not directly associated with visual stimulation, as shown in Figure 5. Such figures enhance the clarity of details such as the time delay

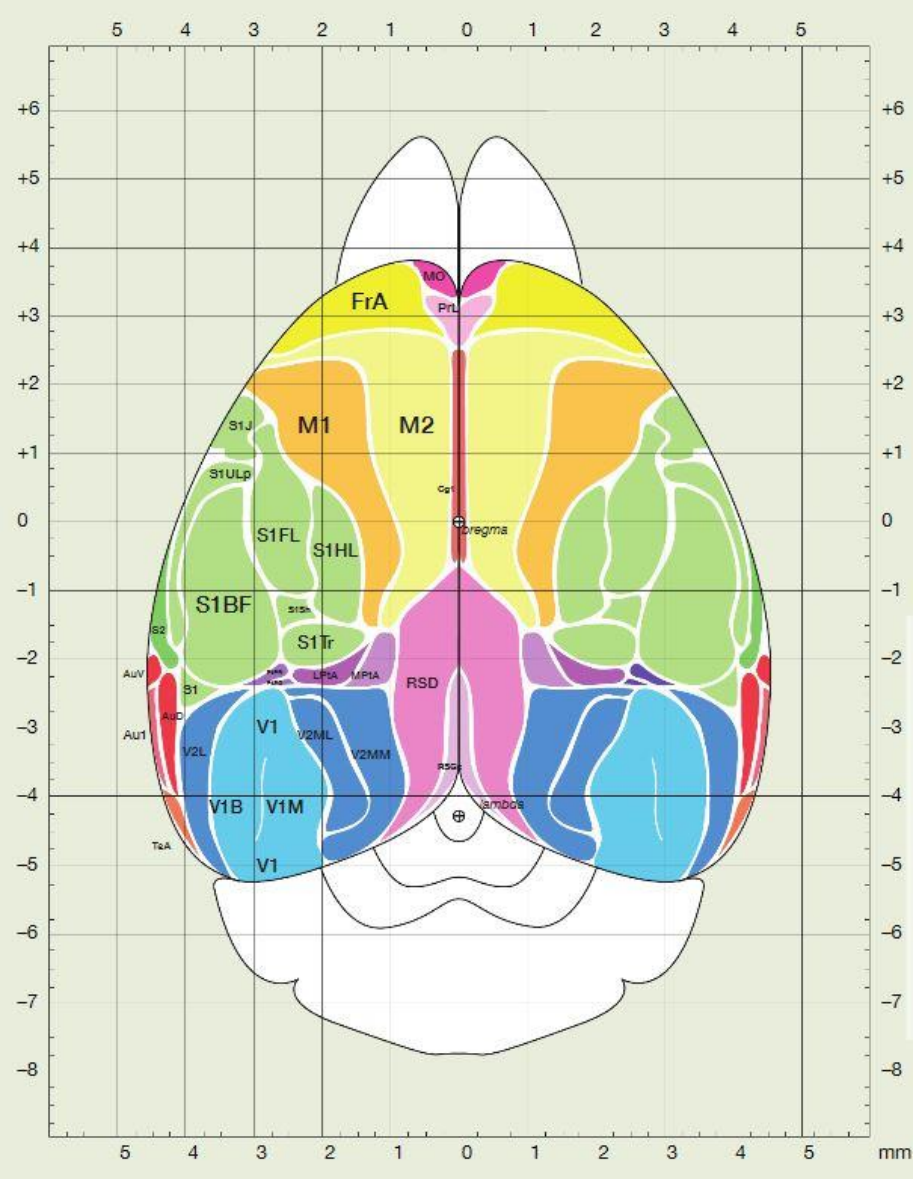

Figure 1: Schematic of the mouse brain, superior view. V1, being the visual cortex, is in light blue; Au1, being the auditory cortex, is in light red (note that throughout this thesis Au1 is simply referred to as "A1"); and S1, being the somatosensory cortex, is in light green. This figure was graciously provided by Michael S. Bobola PhD, a colleague within Mourad group.

between stimulation and neural activation, the comparison in the amplitude of responses between different brain areas, and the levels of residual activity following the spike response.

As mentioned before, temporal averages were employed to reduce the influence of various noises on the signal analysis. In this paper, a temporal average is understood as follows. All of the events with desired parameters (e.g., visual stimulation under isoflurane anesthesia) are averaged in time such that the first point of the result is the mean of the first points of all of the relevant events, the second point of the result is the mean of the second points of all of the relevant events, etc. This process produces a representative timeseries event with generally reduced impacts of noises generated by

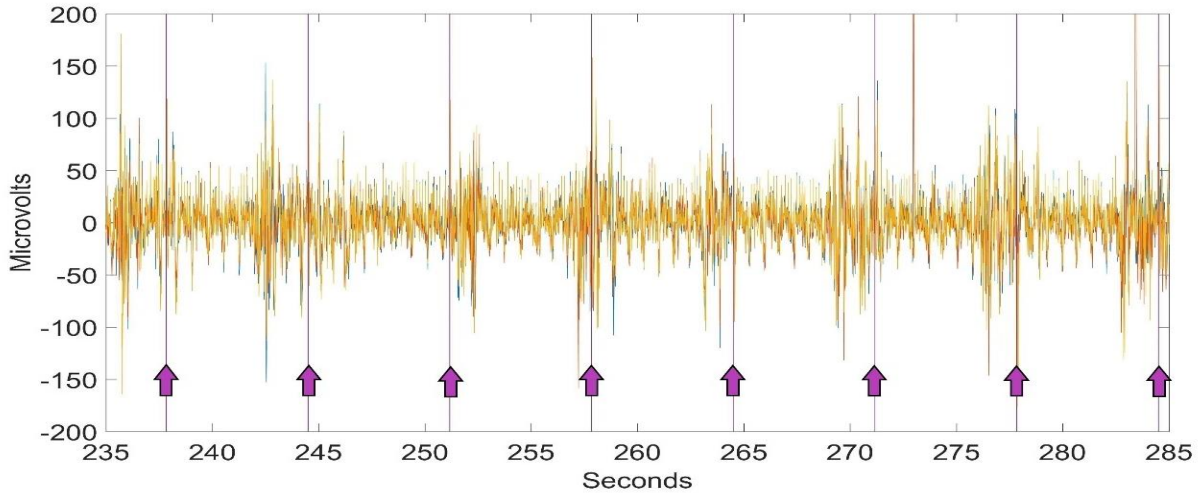

Figure 2: Example timeseries response to visual stimulation. Sample fifty seconds of recording one mouse at brain locations V1 (yellow), A1 (orange), and S1 (blue) bandpass filtered with a second order butter filter between 0.05 Hz and 100 Hz to avoid displaying low frequency effects and to conform with the signal displayed in the CWT figures. The V1 signal appears dominate because it was plotted over the S1 and A1 signals. Visual stimulation is marked with purple vertical lines and associated purple arrows at approximately seven second intervals.

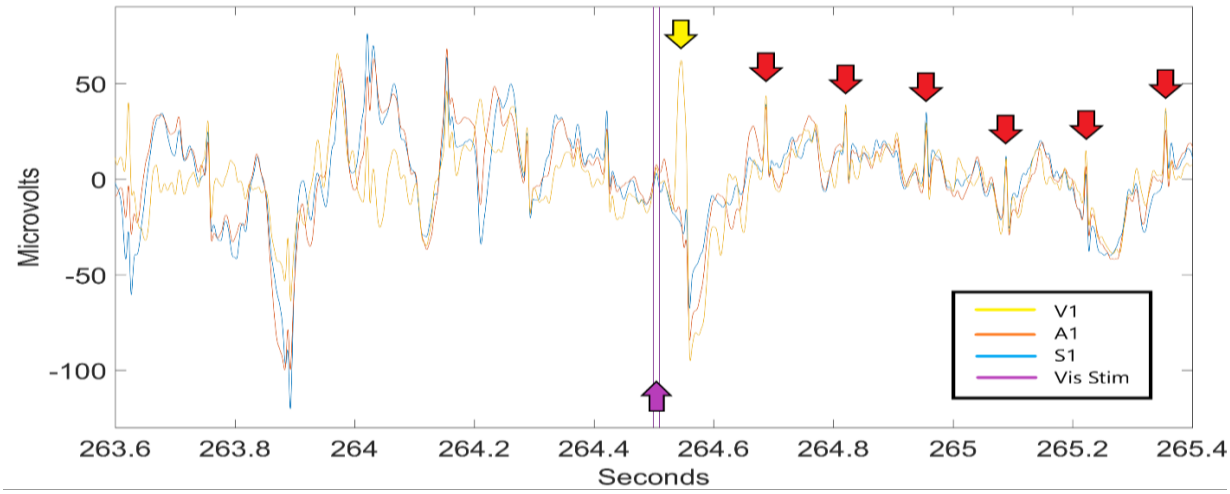

Figure 3: Example timeseries response to visual stimulation. Sample 1.8 seconds of recording one mouse (the same shown in Figure 2) at brain locations V1 (yellow), A1 (orange), and S1 (blue). The visual stimulation is shown in purple and is indicated by a purple arrow. The sharp upward spike in the V1 recording indicated by a yellow arrow is in response to the visual stimulation. Also notice multiple shorter heartbeat-induced spikes shared by all recordings clearly visible between 264.6-265.4 seconds and indicated with red arrows. In addition to heartbeat and activity evoked by stimulation, other electrophysiological phenomena may be present in these signals such as the effects respiration and motor movement.

heartbeat, motor movements, etc., which proves useful for timeseries analysis. An example of temporal averaging is provided in Figure 5. The temporal averaging function is shown below. S_a is the temporal average, $S_1, S_2, \ldots S_M$ are the recordings, M is the number of recordings, and n is the discrete time index.

$$S_a[n] = \frac{S_1[n] + S_2[n] + \cdots + S_M[n]}{M}, for\ n = 0,1,2 \ldots$$

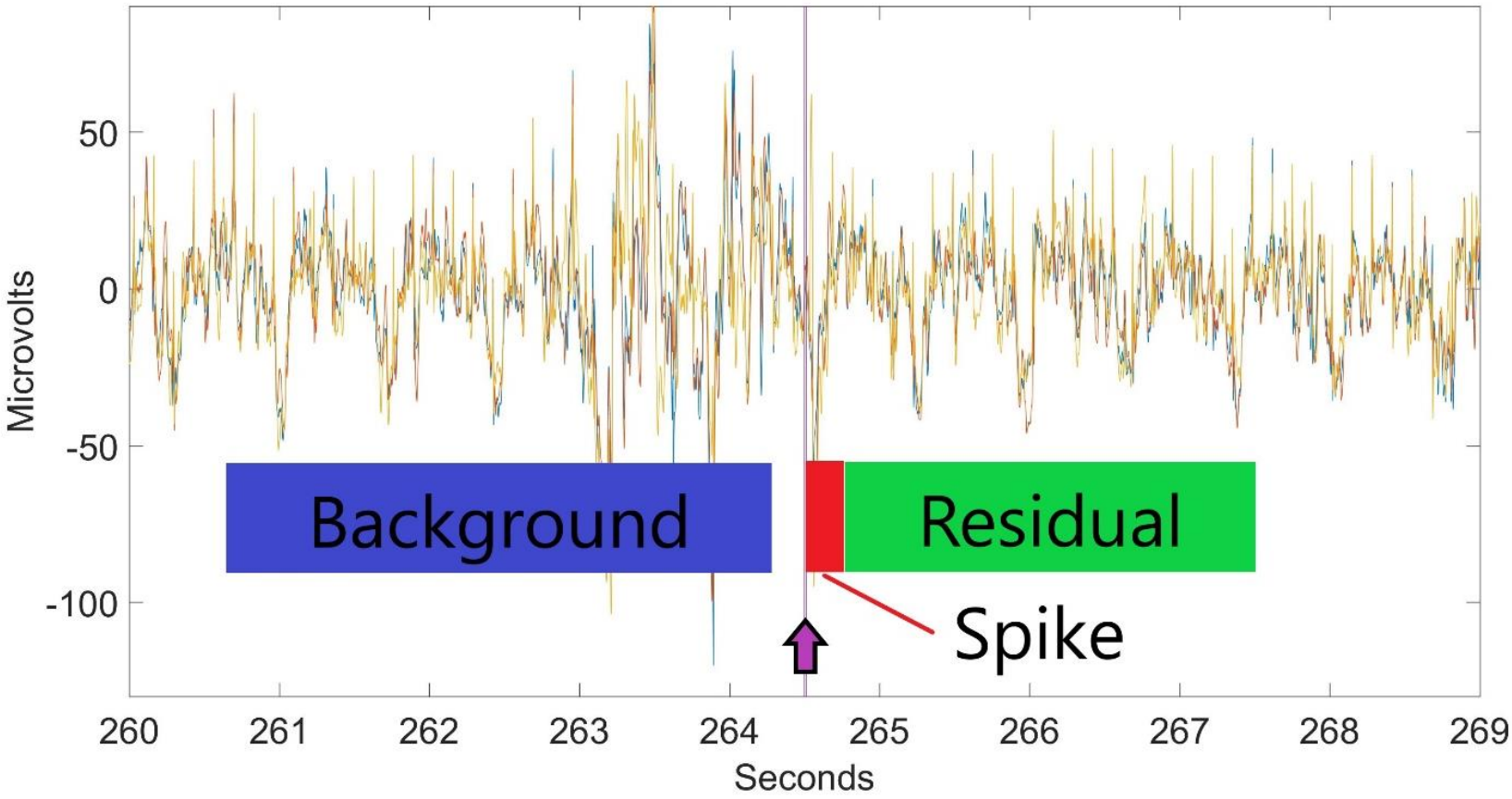

Figure 4: Example timeseries response to visual stimulation. One sample segment (9 seconds) of recording one mouse (the same shown in Figure 2 and Figure 3). The visual stimulation is shown with a purple arrow. The segments of the event are labeled.

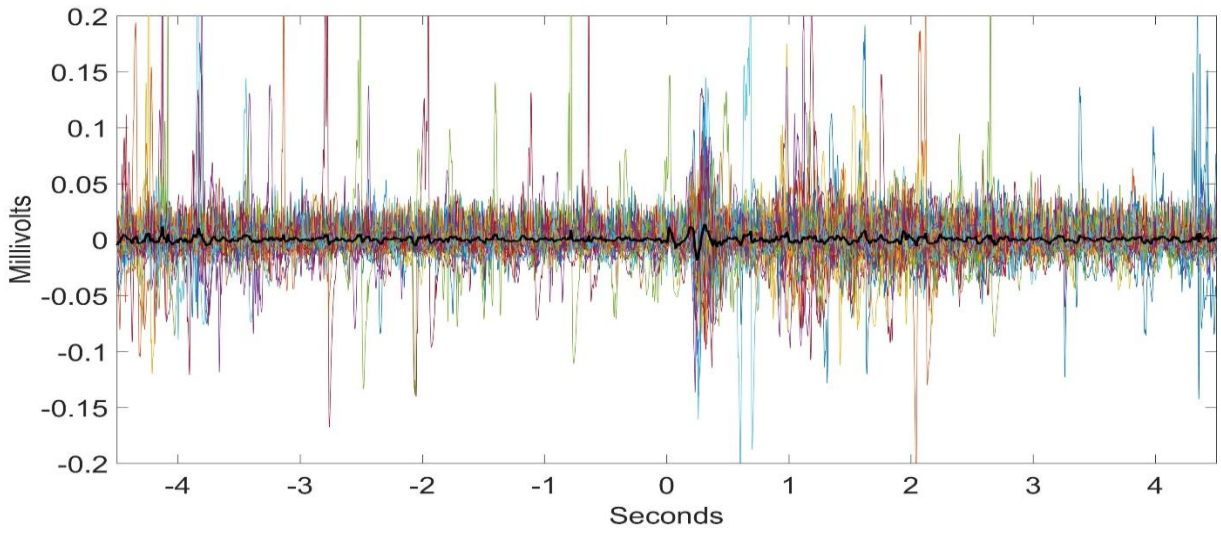

Figure 5: Example temporal analysis of 49 recordings with an ultrasonic stimulus onset at t=0. The thick black line is the average (mean) response.

CONTINUOUS WAVEFORM TRANSFORM

This research utilizes the discrete version of the continuous waveform transform (CWT) to process signals. Where a true spectrogram, which applies the Fast Fourier Transform to segments of signal, would have timeseries resolution too poor to discern meaningful conclusions, a CWT provides a better tradeoff between time and frequency resolution for our purposes. A CWT is essentially comprised of a signal convolved with a predetermined wavelet such that the structures of the signal, specifically structures of the signal which are related to the structure of the wavelet, may be analyzed without wholly sacrificing knowledge of where structures of interest occur in the time domain. In practice, the structures of interest are usually frequencies. To reduce calculation time, recorded signals were downsampled to a sampling frequency of 1000 Hz which, for the purposes of this paper, is a suitable margin above the Nyquist frequency of 200 Hz, i.e. twice the maximum frequency displayed in the CWT figures throughout this paper. (The data was sampled at a higher sampling rate than required to allow for perspective future analysis of higher frequency ranges not considered in this thesis.) The CWT function is shown below. X_w is the CWT output of input function $x(t)$, a is the scale, b is the translational value, $\bar{\psi}(t)$ is the complex conjugate of the wavelet, and t is time.

$$X_w(a,b) = \frac{1}{|a|^{1/2}} \int_{-\infty}^{\infty} x(t)\, \bar{\psi}\left(\frac{t-b}{a}\right) dt$$

In this work, the complex Morlet wavelet was used with a bandwidth frequency of 3 Hz and a center frequency of 2 Hz. The complex Morlet wavelet is analytic which does not allow visibility of negative frequencies, which is desired for reduced analysis complexity, and the complex nature of the wavelet allows phase information of the signal to be analyzed if desired. Phase analysis has not come

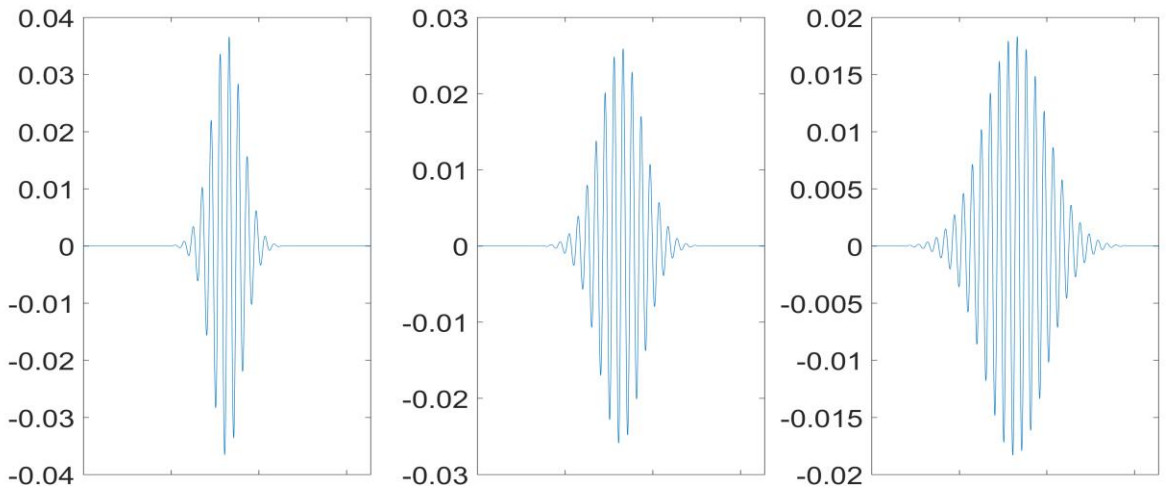

Figure 6: Complex Morlet wavelet with center frequency 2 Hz and bandwidth frequencies of 1.5 Hz, 3.0 Hz, and 6.0 Hz, from left to right, respectively. Only the real parts of the wavelet are shown here. Notice that higher bandwidth frequency wavelets have more cycle repetitions and thus, due to being convolved with the recorded signal in the CWT, provide better frequency resolution at the expense of time resolution, and lower bandwidth frequency wavelets have fewer cycle repetitions and thus provide better time resolution at the expense of frequency resolution. The y-axes are scaled for visualization purposes.

into play in this current thesis work so the absolute value of the complex result is taken, but the computer code is established for such investigation in the future. Where the complex Morlet wavelets offers greater frequency resolution at the expense of time resolution in comparison with other common wavelets such as the bump wavelet and the Mexican hat wavelet, timeseries analysis provides enough understanding of the various timeseries attributes that it is reasonable to choose a wavelet favoring frequency resolution. The complex Morlet wavelet function $\psi_{complex\ Morlet}(t)$ is shown below, where f_b is the bandwidth frequency, f_c is the center frequency, and t is time.

$$\psi_{complex\ Morlet}(t) = \left((\pi f_b)^{-1/2}\right)\left(e^{-i2\pi f_c t}\right)\left(e^{-t^2/f_b}\right)$$

Within the bounds of the complex Morlet wavelet, the bandwidth frequency of 3 Hz was chosen as a convenient medium between the higher time resolution that a lower bandwidth frequency would provide, at the expense of frequency resolution, and the higher frequency resolution that a higher bandwidth frequency would provide, at the expense of time resolution. Examples of the real parts of the complex Morlet wavelets at different bandwidth frequencies are shown in Figure 7. When Figure 8A, an example CWT with a bandwidth frequency of 1.5 Hz, and Figure 8C, the same example CWT with a bandwidth of frequency 6.0 Hz, are compared with Figure 8B, the same CWT with a bandwidth frequency of 3.0 Hz, the differences become apparent. The 1.5 Hz bandwidth frequency causes the result to be smeared vertically along the frequency axis, indicative of its weaker frequency resolution. Similarly, the 6.0 Hz bandwidth frequency causes the result to be smeared horizontally along the time axis, indicative of weaker time resolution. Once a CWT is generated for an event within the signal, a variant of an average is taken across all relevant event CWT's to produce a CWT with a general reduction in noise. The following section on global cluster analysis explains how the averages were masked to produce the results which are analyzed in this paper.

GLOBAL CLUSTER CORRECTION

Global cluster correction is a method by which a dataset may be processed to better ensure that results are truly statistically significant, a need facetiously yet sagely expressed by Bennett *et al* after performing a successful study where "the task administered to the [dead] salmon involved completing an open-ended mentalizing task" (Bennett CM 2011). The analysis in this study was modeled after the analysis provided by Darvas *et al* (Darvas F 2016). After the CWT was taken for each event, the median of the CWT results was taken and converted into a Z-score (the difference between the sample and mean divided by the standard deviation) where the mean and standard deviation of the Z-score were calculated from the CWT results ranging from 0.2 seconds to 3.8 seconds before the stimulation onset for each frequency step. This range was chosen to avoid influence of the stimulation onset which, depending on filtering practices, may exist before the stimulation onset and to avoid influence of CWT edge effects of the event segments. The Z-score formula is shown below where Z is the Z-score of the sample value X, μ is the mean of the sample population, and σ is the standard deviation of the sample population.

$$Z = \frac{X - \mu}{\sigma}$$

The Z-score is then converted into a color map and masked based on a t-statistic (which is calculated in a similar way as the Z-score except for an additional multiplication by the square root of the number of values in the population) and then masked again to show only the values of 2 standard deviations (except as noted for visualization purposes in Figure 8 and Figure 9) or greater above the mean in clusters which passed the global cluster correction. The choice to mask at 2 standard deviations is patterned after recent studies by Ikegaya group where 2 standard deviations departure from baseline was provided as evidence of visual stimulation residual effects (Minamisawa G 2017, Funayama K 2015). Although a 2 standard deviation mask is, for most of the visual stimulation CWT figures, weaker than necessary for reader to gain insights, this standard alone was selected to provide consistency between the visual stimulation and ultrasonic stimulation CWT figures. The t-statistic formula is shown below where the t-statistic $t_{statistic}$ is calculated from the mean μ, standard deviation σ, and number of samples N, of populations a and b.

$$t_{statistic} = \frac{\mu_a - \mu_b}{\sqrt{{\sigma_a}^2 / N_a + {\sigma_b}^2 / N_b}}$$

Figure 9 shows the results of standard deviation CWT masking at 2, 4, and 8 standard deviations, respectively. The scale is also shown in Figure 9D. To generate the t-statistic mask, a t-statistic was calculated from the Z-score (specifically, the Z-score which existed before the median was taken and is a normalization of the raw CWT data) in the ranges -3.8 seconds to -0.4 seconds and -0.4 seconds to 3.0 seconds, being Z-scores before and after the stimulation onset. An example result of the masking when the t-statistics are generated from the raw CWT data instead of the normalized Z-scores is shown in Figure 10B; when compared with Figure 10A less activity is visible, particularly in the 2-3 second range, which illustrates the difference in results when normalization for each frequency step is neglected. This t-statistic as generated from the Z-score was then transformed into logical maps of

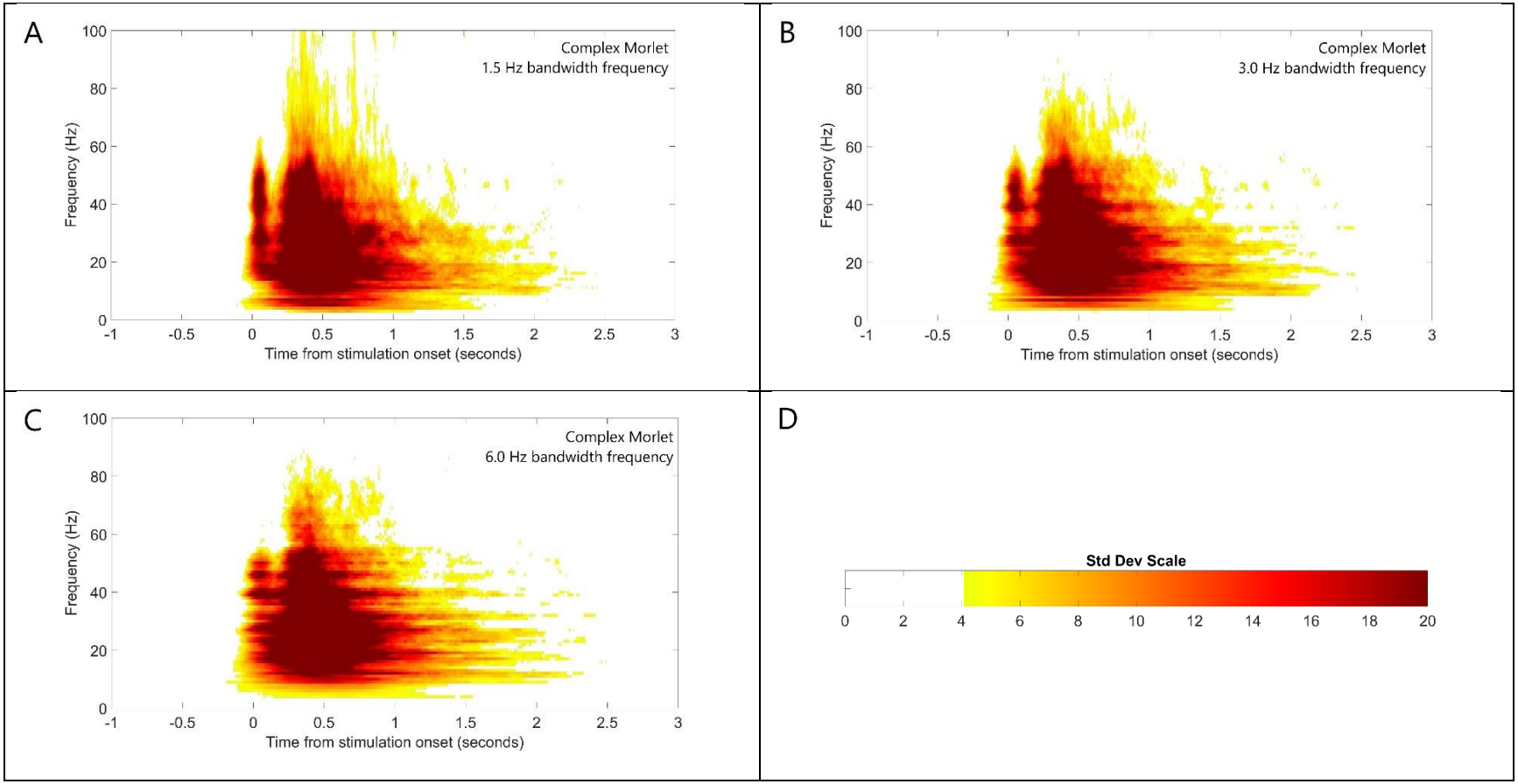

Figure 8: Example results of complex Morlet, center frequency 2.0 Hz, 100 permutations used for global cluster correction t-statistic mask calculation and standard deviation mask of 4 standard deviations plotted from 1 second before to 3 seconds after the stimulation onset at t=0. (In this example case, visual stimulation is used.) A mask of 4 standard deviations is used to draw attention to the tradeoffs between time resolution and frequency resolution. Across the y-axis, figures are plotted from 0 Hz to 100 Hz with the upper frequency bound being at, given the lack of uniformity of gamma band upper bounds across the literature, the approximate upper end of the gamma band upper bound range. (A) Bandwidth frequency of 1.5 Hz provides greater time resolution at the expense of frequency resolution as made evident by the vertical smearing in comparison to 3.0 Hz bandwidth frequency, as seen particularly in the upper frequency ranges between about 0 and 1 seconds. (B) Bandwidth frequency of 3.0 Hz was selected for the analysis performed in this paper because it provided an ideal tradeoff between time and frequency resolutions as compared to the results seen for bandwidth frequencies of 1.5 Hz and 6.0 Hz. (C) Bandwidth frequency of 6.0 Hz provides greater frequency resolution at the expense of time resolution as made evident by the horizontal smearing in comparison to the 3.0 Hz bandwidth frequency, as seen particularly in the transition from dark red (approximately 20 standard deviations) to light red (approximately 15 standard deviations) at several frequencies. (D) Power color scale in terms of standard deviations above the background mean for each frequency. Note that some areas of the figure saturate the scale which was capped at 20 standard deviations from the mean for figure visibility purposes. (More calculation description may be found in the GLOBAL CLUSTER CORRECTION section).

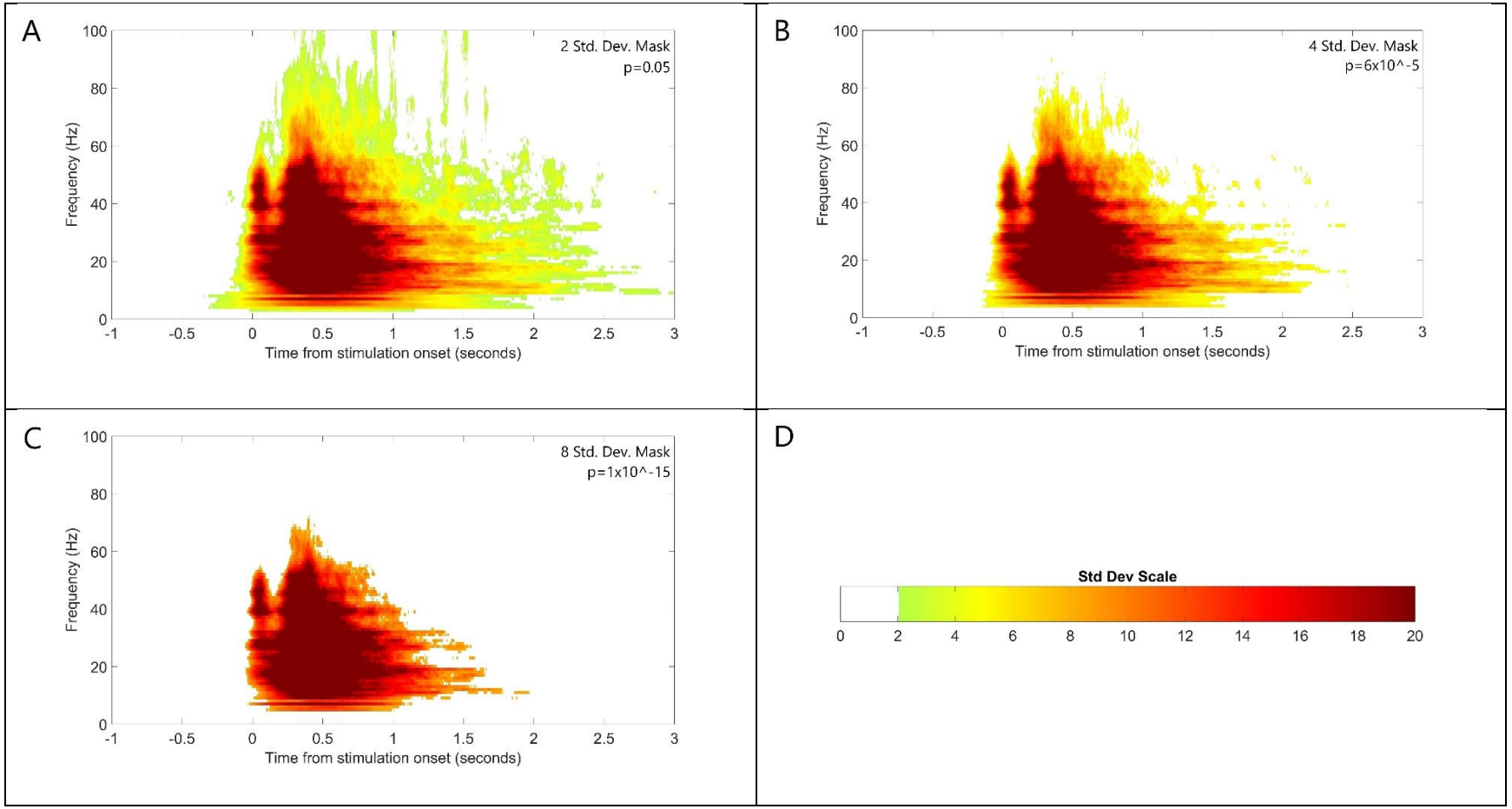

Figure 9: Varying standard deviation masks on an example CWT calculation of ECoG, bandwidth frequency 3.0 Hz. (A) 2 standard deviations, which is the level chosen for use in this study. (B) 4 standard deviations. (C) 8 standard deviations, which shows the most compact signal. (D) Standard deviations from the mean power of the signal prior to stimulation onset.

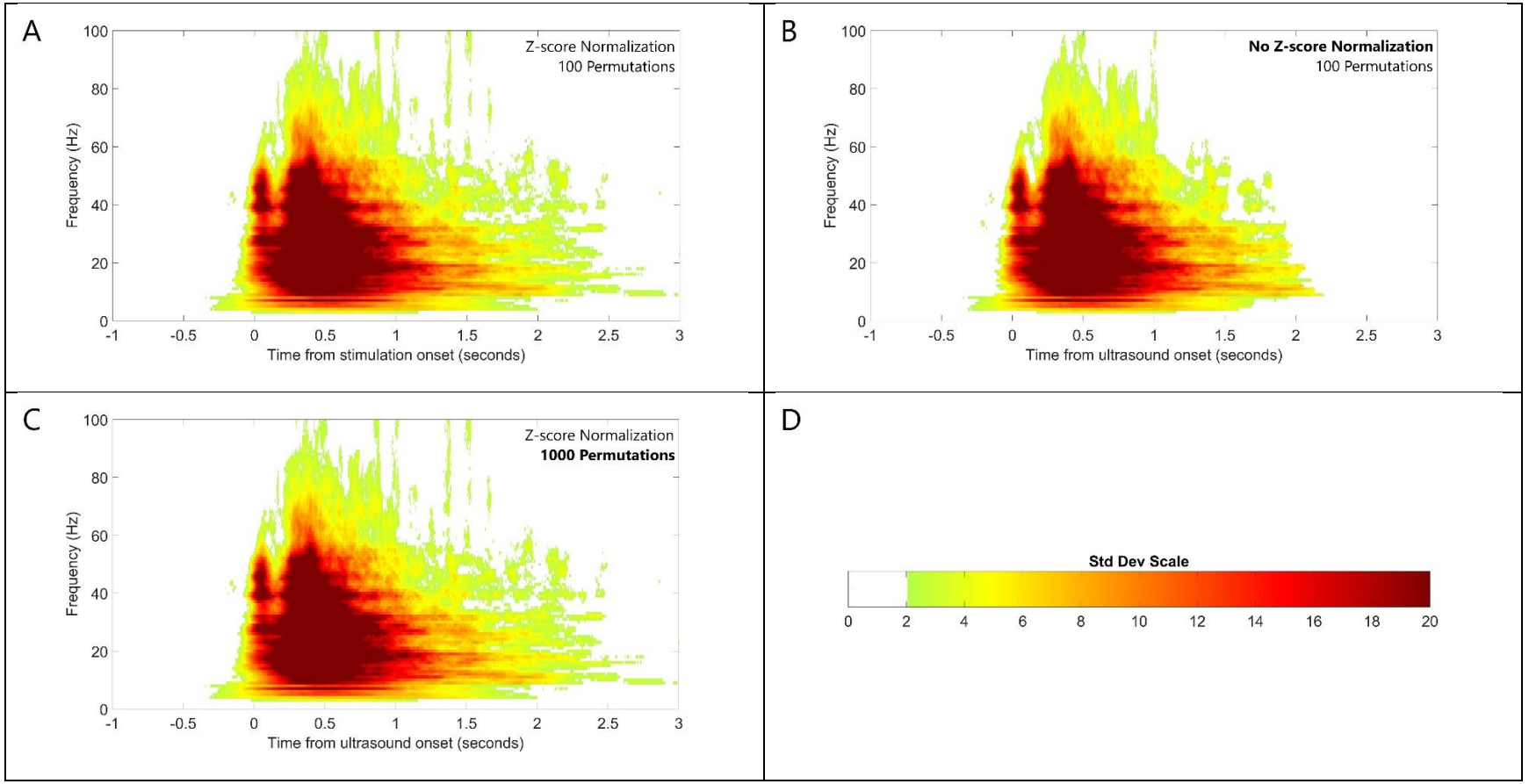

Figure 10: Example CWT calculation of ECoG, bandwidth frequency 3.0 Hz with and without Z-score normalization and with varying numbers of permutations. (A) Z-score normalization and 100 permutations, which represent the choices used throughout this study and a duplicate of Figure 9A. (B) Z-score normalization omitted from mask calculation; raw CWT values were used to generate the t-statistics which are used to generate the global cluster correction mask. Several differences are noticeable in comparison with inset A, such as the lack of activity in the 2-3 second range. (C) Increased algorithmic permutations from 100 to 1000. Because the differences in the results are minor, the option of 100 permutations was selected for use in this paper to speed calculation time. (D) Standard deviations from the mean power of the signal prior to stimulation onset.

values exceeding or not exceeding a threshold, which in this case was 2. The Z-score maps for pre- and post-onset were then permuted 100 times (unless stated otherwise) and the logical maps of the permutated data calculated. (Find more on permutation in the PERMUTATION TEST section, below.) The largest cluster (regardless of shape) of the permuted data, being the largest contiguous set of elements exceeding the threshold, was recorded for each permutation. If a cluster from the original Z-score data, after being transformed into a t-statistic, exceeded the size of 95% of the permutation-produced maximum area clusters then the cluster of the original data was not masked. Figure 10A is an example CWT with 100 permutations used to create the t-statistic mask and Figure 10C is the same CWT except that 1000 permutations were used to create the mask. Because the results are quite similar and thus either option would suffice for the purpose of this paper, the 100 permutations option was selected as the standard to reduce calculation time.

PERMUTATION TEST

Permutation tests are often a convenient way to determine if a result is significant without in-depth knowledge of various formal statistics tests and their specific assumptions and limitations. Because a true permutation test, which requires every permutation of the data be considered, may have impractical calculation times, this research used an approximate permutation test which samples several, but not all, random permutations.

In the case of GLOBAL CLUSTER CORRECTION, as described above, the pre-stimulation onset and post-stimulation onset Z-score maps was permuted such that what was assigned pre-stimulation onset data or post-stimulation onset data was randomly reassigned to the other category. That new, permuted dataset was analyzed for clusters and then the largest cluster of each iteration was recorded. With this data, significance of clusters in the original data could be determined by comparing it with the distribution of largest cluster sizes from the randomly permuted data.

Permutation tests can also be used to analyze means between two populations. The collection of data is permuted and re-separated into two populations, the means are taken of each and the difference in the means is recorded. Repeating this process many times builds a distribution for the difference in the means between the two populations. The percentage of cases above or below the difference of the means of the original two populations generates the *p* value, thus providing an understanding of how statistically significant the means of the two original populations are. This analysis was used in this research on distributions which were assumed to have non-equal variances and were assumed to be non-parametric, a combination of distribution traits which prove difficult to handle with traditional statistics tests.

VISUAL STIMULATION OF HEALTHY MICE

Mice were visually stimulated to generate control data. This control data will be compared with data generated from ultrasonic stimulation of mice in the next section.

SETUP

To generate control data, mice were put under isoflurane, a type of anesthesia, and situated in a stereoscope on top of a heating pad. ECoG electrodes were placed in the V1, A1, and S1 brain regions and an LED light programmed to blink for on for 10-100ms periodically every several seconds was placed near the mouse's eye. (ECoG was employed instead of EEG in order to collect clearer signals from the brain for this preliminary study.) The brain signals were then recorded from the electrodes while the anesthesia levels were monitored in an effort to maintain an approximately constant brain state throughout the recording process.

RESULTS

Temporal averages were used to minimize activity not directly associated with visual stimulation, as shown in Figure 11. Such figures enhance the clarity of details such as the time delay between stimulation and neural activation, the comparison in the amplitude of responses between different brain areas, and the levels of residual activity following the spike response. The strength of the response in V1 as compared to A1 and S1 confirms that the visual stimulations are successful and provides a control for studies involving ultrasonic activation. Energy of both the spike and the residual activity of V1 is also measured in Figure 12 as a control for ultrasonic stimulation studies. It is noted that the mean energy for both the spike and the residual and for both isoflurane and medetomidine increased with respect to background neural activity. This "residual" following the visual stimulation, at least in the case of the brain under isoflurane, is thought to be indicative of calcium (Ca^{2+}) slow waves which are waves of calcium-related activity which traverse regions of the brain much more slowly than does neuronal activity. The important relationship between slow waves and healthy sleep is studied and effort has been directed toward the enhancement of slow waves (Bellesi M 2014). It is also noted that some of the data resides below zero, indicating that not all stimulations trigger activity with respect to background. This is consistent with findings throughout the literature which show that ultrasound can be used to either stimulate or suppress neural activity (Yoo SS 2011).

Corticothalamic calcium waves have been observed by Stroh *et al.* in response to visual stimulation of mouse brain *in vivo* (Stroh A 2013). While it is widely accepted that neurons can trigger each other to fire at high speeds, Stroh *et al.* found that calcium slow waves propagate at approximately 37 mm/s through the cortex. Such local brain calcium state changes after an initial impulse appear to be linked to the residual electrical activity like that shown in this paper for mice under isoflurane. Isoflurane, it should be noted, puts the mouse in a non-REM sleep brain state where slow waves occur, as has been demonstrated by fMRI study of slow waves (Schwalm M 2017). Figure 13A, Figure 13B, and Figure 13C display averaged recordings of V1, S1, and A1, respectively, in visually stimulated mice where the onset of the flash of light occurs at *t=0*. It is evident in all figures that the visual stimulation evokes an initial response, being the spike previously discussed, followed by the slow waves. The spike is more pervasive in V1 than S1 or A1, as expected. The slow waves offer more to ponder, seeing that S1, and to a lesser extent A1, appear to have a stronger slow wave response in the range of about 7 Hz to about 22 Hz than does V1 in the vicinity of *t=0.5*. Despite the differences in the slow wave onset, it is noted that in A1 and S1 that slow waves taper off into masked territory at roughly the same time for most frequencies. The finding is reasonable, seeing that A1 and S1 are in close proximity, and it may suggest that the strength of the slow wave onset is not linearly related to slow wave duration. All this being said,

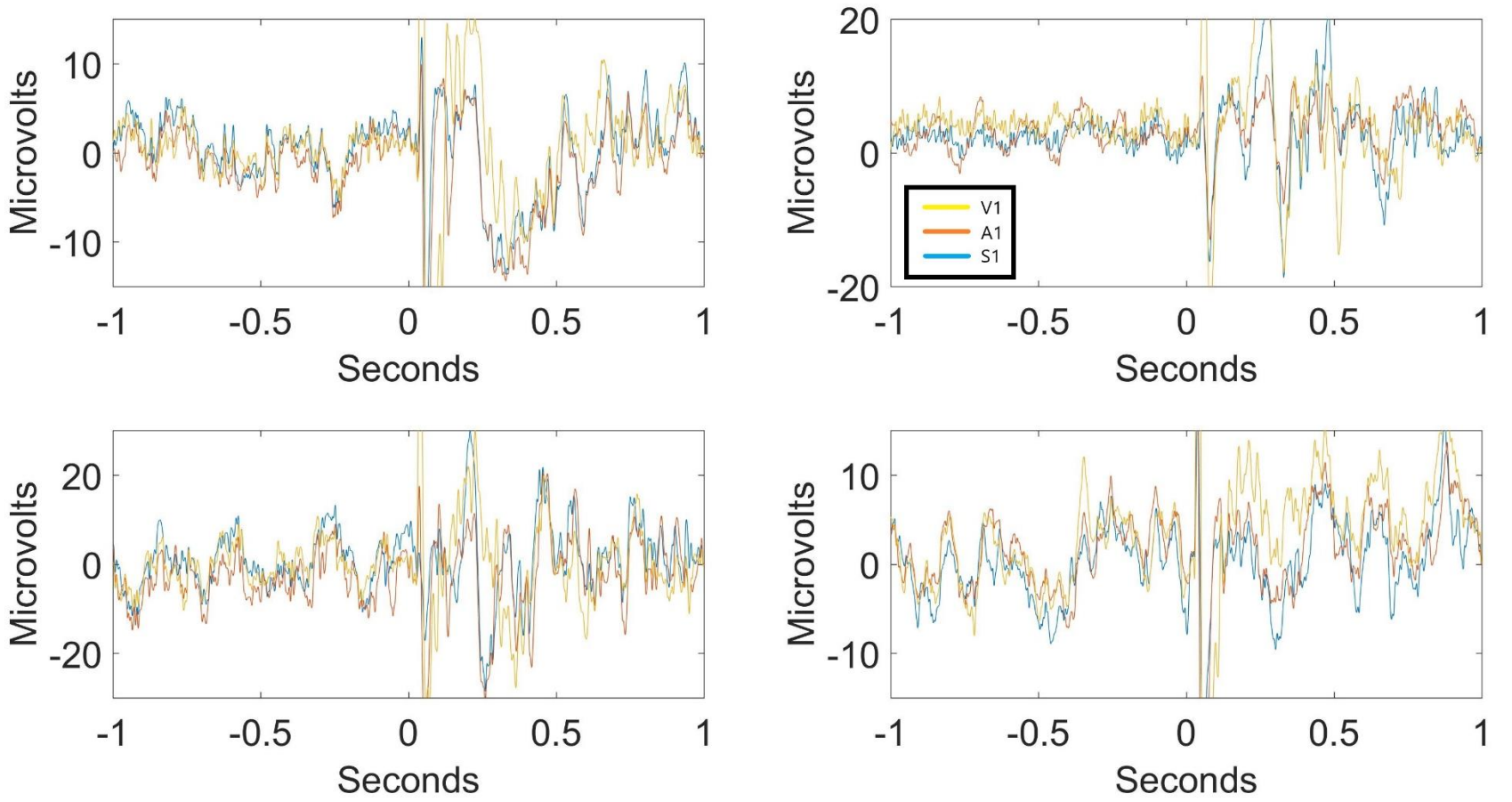

Figure 11: Example average timeseries response to visual stimulation under isoflurane. Two seconds of recording four mice at brain locations V1 (yellow), A1 (orange), and S1 (blue) under isoflurane anesthesia, filtered with a bandpass second order Butter filter from 0.05 Hz to 100 Hz to keep consistency with the CWT visualizations. Note that the voltage axis varies by window. The onset of the visual stimulation onset is at t=0 with the evoked spike occurring shortly after and extending out of the plot window in both the positive and negative directions for V1 in all cases and for other brain areas in some cases. The energy of the signal after the spike is stronger than before the spike as manifested by the increased amplitude oscillations—this is indicative of slow wave activity.

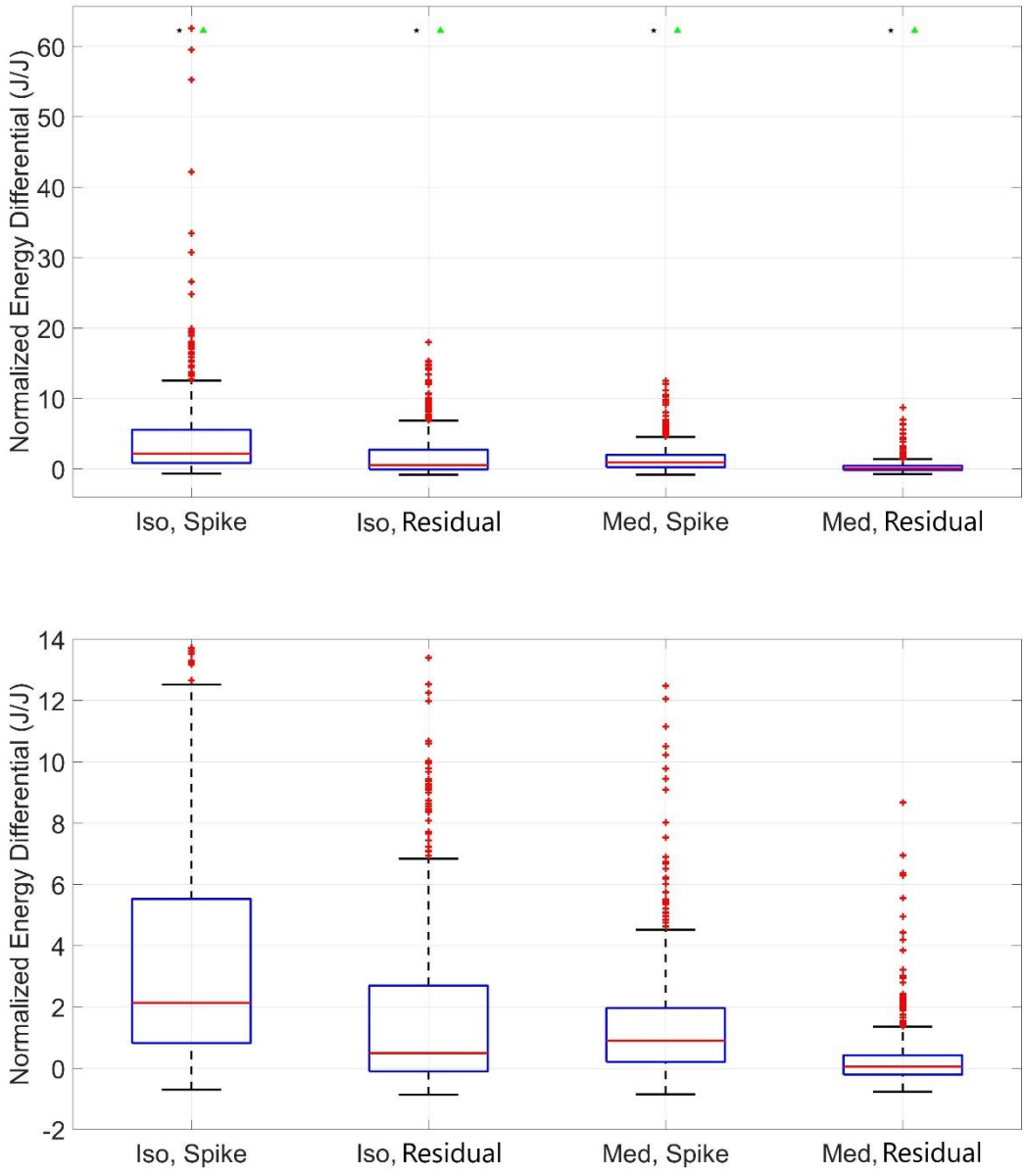

Figure 12: Difference in energy between background (0.2-3.8 seconds before stimulation onset) and spike response (0.0-0.2 seconds after stimulation onset) as normalized by background energy, and difference in energy between background (0.2-3.8 seconds before stimulation onset) and residual response (0.2-3.0 seconds after stimulation onset) as normalized by background energy for each event across 9 mice assembled as box-and-whisker plots under isoflurane and medetomidine. (Refer to Figure 4 for energy segmentation visualization.) Means were determined to be statistically above zero as determined by the non-parametric Wilcoxon signed rank test and as indicated by black stars and accompanying upward pointing green triangles. A significance level of 5% was chosen, in alignment with academic customs. This non-parametric test was selected to free the analysis from concerns arising from unknown distributions of data. In the zoomed-in version of the data (lower image), it becomes evident that some events generate less energy during the spike or during the residual than during the background because some of the data extend below zero.

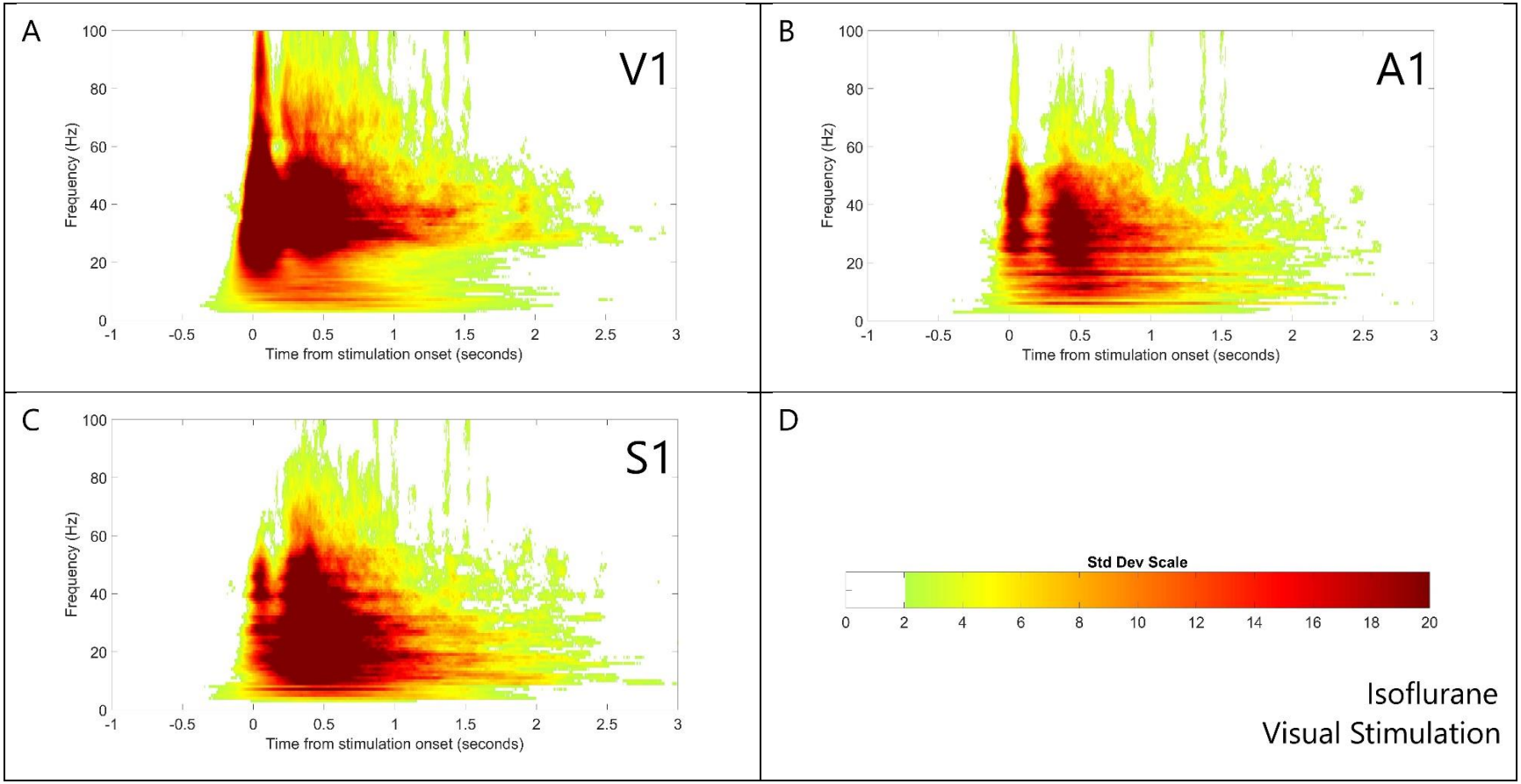

Figure 13: CWT recordings of ECoG, bandwidth frequency 3.0 Hz, standard deviation mask at 2, with global cluster analysis of 8 mice under isoflurane visually stimulated. (A) V1 response exhibits a strong initial spike associated with the light stimulation followed by slow waves. (B) A1 exhibits a weaker initial spike due to the light as well as bleed-through from the visual cortex and weaker slow waves in comparison with V1, as expected. (C) S1 exhibits a weaker initial spike than V1 (also due to bleed through) but displays apparently stronger slow waves. (D) Standard deviations from the mean power of the signal prior to stimulation onset.

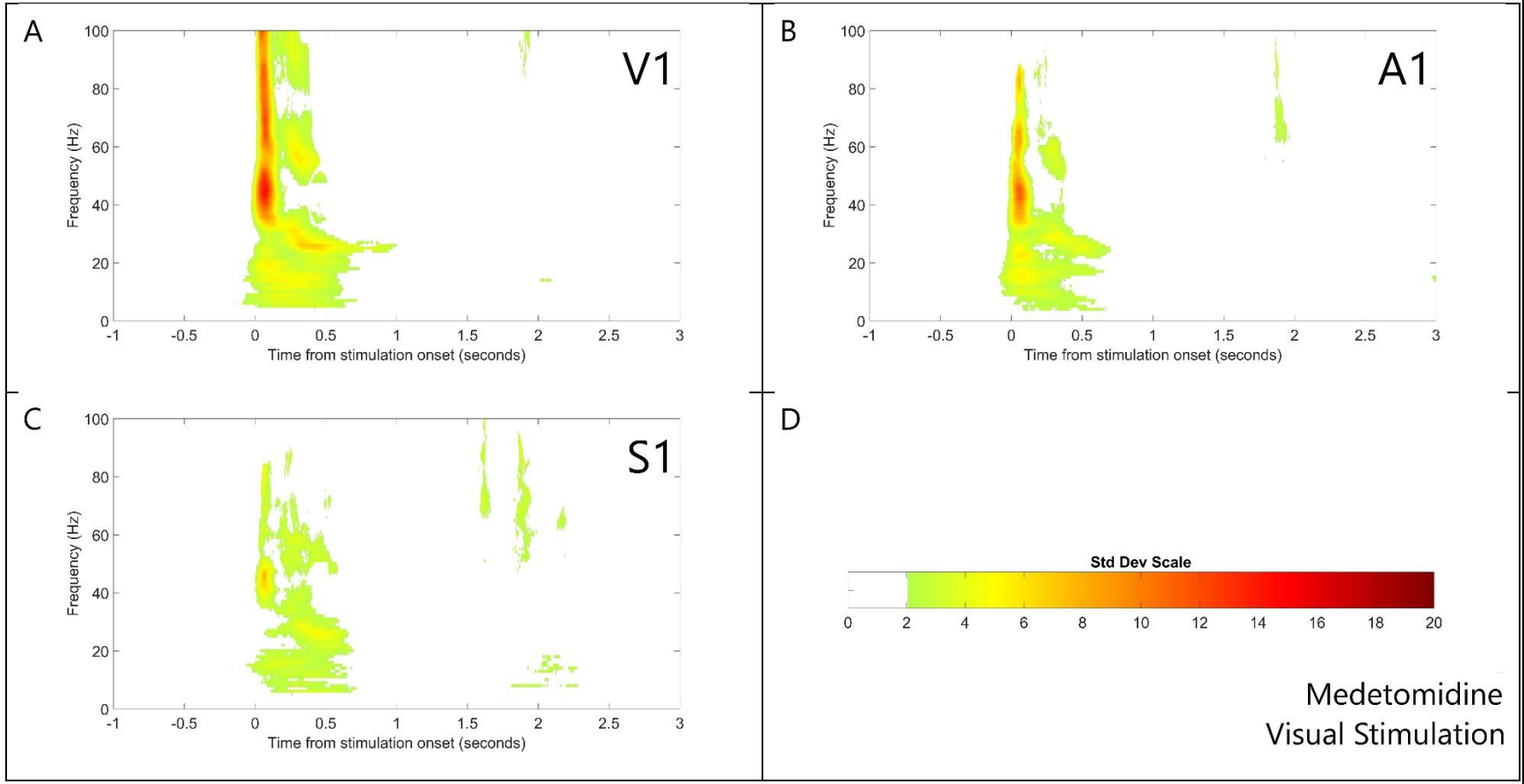

Figure 14: CWT recordings of ECoG, bandwidth frequency 3.0 Hz, standard deviation mask at 2, with global cluster analysis of 8 mice under medetomidine visually stimulated. (A) V1 response exhibits a strong spike followed by weak residual activity. (B) A1 exhibits a weaker spike and weaker residual activity in comparison with V1, as expected. (C) S1 exhibits a weaker spike than both V1 and Z1 and weaker residual activity in comparison with V1, as expected. (D) Standard deviations from the mean power of the signal prior to stimulation onset.

there is also a strong chance that the wires at each brain region are long enough to pick up signal "bleeding" from other brain regions, especially regions of close proximity like the ones being studied here; this is to say that the evoked activity of V1 likely contributes to the responses of A1 and S1. Furthermore, whether these more detailed phenomena will hold true under a larger sample size remains to be seen, per the nature of this preliminary study.

Slow waves are not present in all brain states, however. The mice were sedated with medetomidine such that their brains would take to their awake states and then recordings were taken in the same way that they were done under isoflurane anesthesia. The differences from the isoflurane scenarios are striking, as depicted in Figure 14. To begin, the spike in V1 under medetomidine as shown in Figure 14A does not demonstrate nearly as much activity in the roughly 15 Hz to 35 Hz range as does the V1 under isoflurane as shown in Figure 13A, and slow waves under medetomidine are drastically weakened. The weakening of the slow waves is evidence for the effects that brain state caused by the differential effects of anesthesia (isoflurane) versus sedative (medetomidine)have on neural responses to stimuli. In the case of S1 the changes are the starkest because the little activity left unmasked is weak as shown in Figure 14C. In Figure 14B we see that A1 under medetomidine appears as a weaker version of V1 under medetomidine, much like A1 under isoflurane appears, except for in the previously mentioned lower frequency slow waves, as a weaker version of V1 under isoflurane, which is consistent with the general idea that brain activity would be greatest in the brain regions most closely associated with the stimuli.

ULTRASONIC STIMULATION OF HEALTHY MICE

Mice were ultrasonically stimulated and the data collected was compared with the visual stimulation data. The similarities were considerable yet left room for considerations of subtle differences in the mechanics of the effects between ultrasonic and visual stimulation.

SETUP

Having considered the control data with visual stimulation, we move on to ultrasonically stimulated healthy mice. The experimental setup was much the same, except with the application of pulsed and focused ultrasonic stimulation through the skull, directly into V1 instead of visual stimulation via the retina of the eye. The ultrasound was set with a carrier frequency of 2.00 MHz and a pulse repetition frequency of 1050 Hz. The number of pulses within each stimulation burst was varied experiment to experiment, and the time between bursts was set for several seconds to allow slow waves to dissipate. All results are drawn from small sample sizes and must be considered as preliminary findings.

RESULTS

Four timeseries response example time averages of mice under isoflurane are displayed in Figure 15, two with 10 pulses within each burst and two with 100 pulses within each burst. The burst counts were chosen to provide similar stimulation duration to that of the visual stimulation. These timeseries responses look markedly different than the timeseries responses due to visual stimulation as seen in Figure 11, and the change in y-axis scale and the location of zero amplitude on the graph should

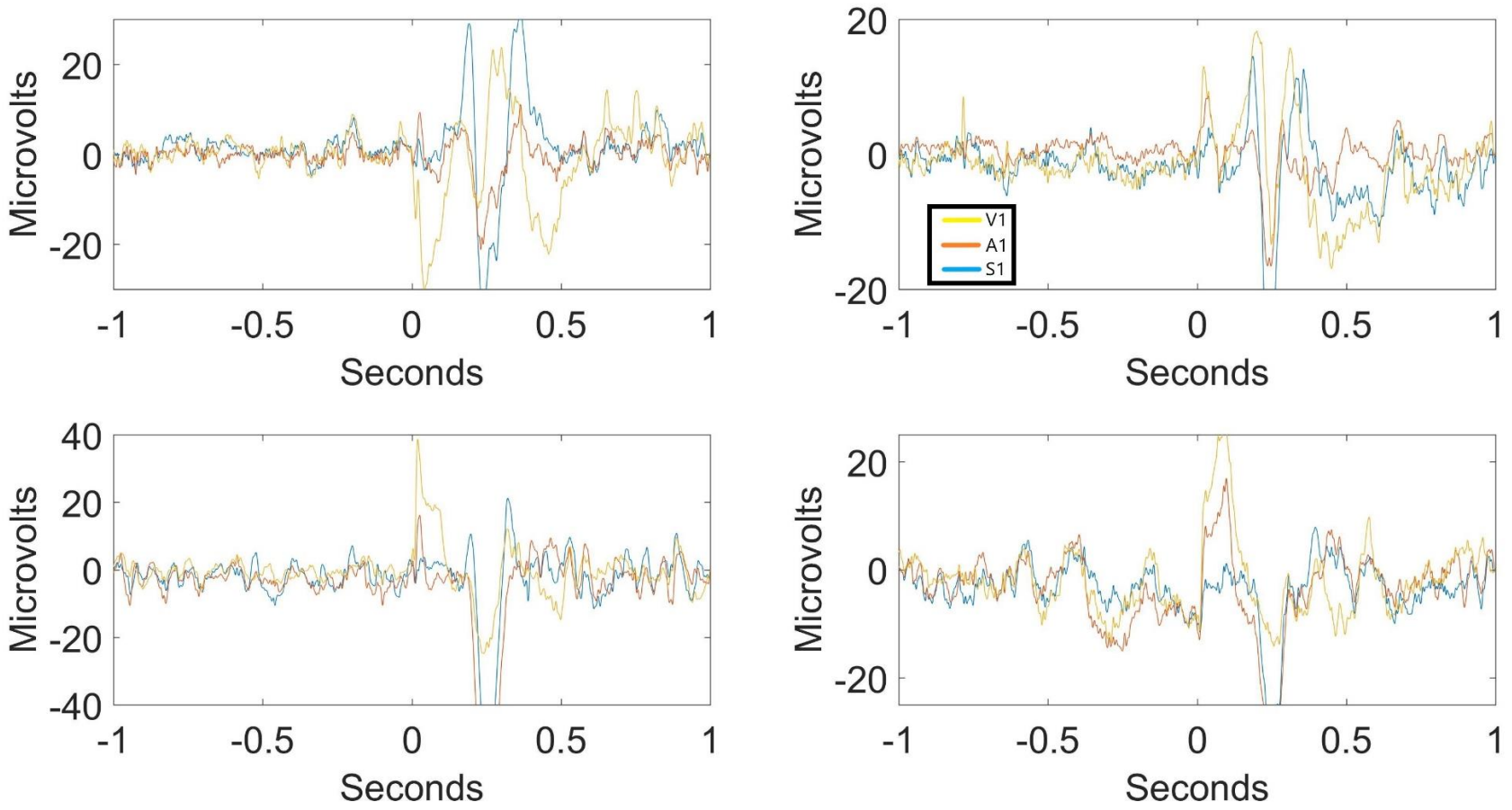

Figure 15: Example average timeseries response to ultrasonic stimulation of V1 under isoflurane. Two seconds of recording four mice at brain locations V1 (yellow), A1 (orange), and S1 (blue) under isoflurane anesthesia, filtered with a bandpass second order Butter filter from 0.05 Hz to 100 Hz to keep consistency with the CWT visualizations. The onset of the ultrasonic stimulation event is at t=0 with the evoked spike occurring shortly after. The stimulation of the upper two subplots lasts 9.5 ms, being 10 bursts of 2.00 MHz US at a pulse repetition frequency of 1050 Hz. The stimulation of the lower two subplots lasts 95 ms, being 100 bursts of 2.00 MHz US at a pulse repetition frequency of 1050 Hz. The energy of the signal after the spike is stronger than before the spike as manifested by the increased amplitude oscillations.

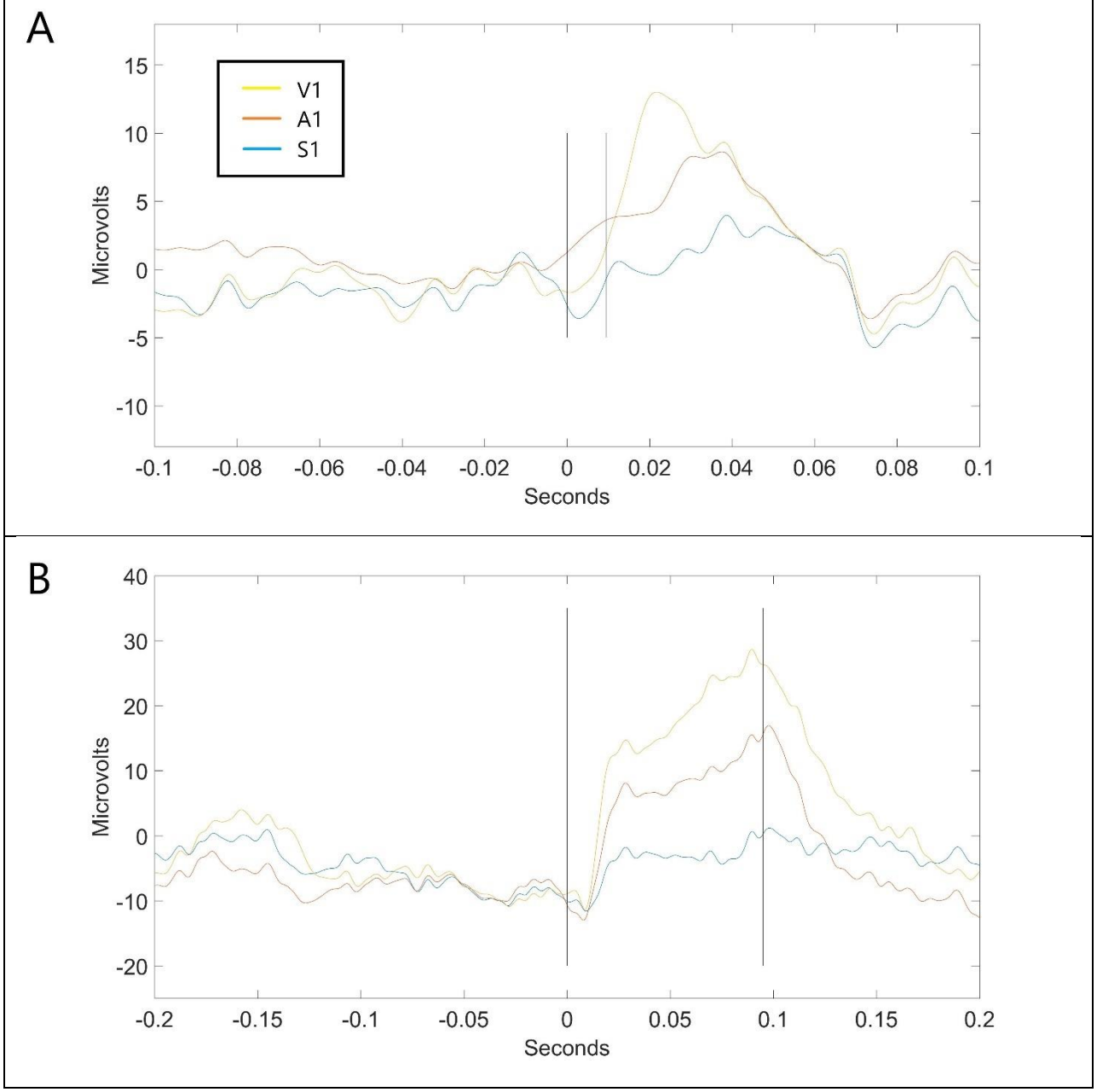

Figure 16: Example average timeseries responses to ultrasonic stimulation of V1. Two seconds of recording a mouse at brain regions V1 (yellow), A1 (orange), and S1 (blue). The ultrasonic stimulation duration is marked by the vertical black bars. Notice that the x- and y-axes differ for visualization purposes. Signals bandpass filtered between 0.05 and 100 Hz to represent CWT visualizations (A) The stimulation lasts 9.5 ms, being 10 bursts of 2.00 MHz US at a pulse repetition frequency of 1050 Hz. Observe that the activity of V1 and, to a lesser extent, A1 continue to rise after the ultrasound cessation which provides evidence of neural activity evoked by a brief ultrasonic stimulation. (B) The stimulation lasts 95 ms, being 100 bursts of 2.00 MHz US at a pulse repetition frequency of 1050 Hz. Observe that the activity of V1 and A1 abruptly fall after the cessation of ultrasound. This suggests that ultrasound may evoke and sustain neural activity beyond the natural steady state.

be duly noted. Where the light-stimulated spikes within the visual cortex (Figure 13) were clean, sharp, and appear shortly after the stimulation onset and followed by slow wave activity of weaker amplitude, the ultrasonically stimulated spikes generated within the visual cortex by application of ultrasound to the visual cortex are less clear and are followed by slow wave activity of stronger amplitude than the spike. The slow wave activity does, in some cases, appear curiously stronger in amplitude for brain regions other than V1. Zooming in on two example time averaged onsets in displays more clearly when the burst of ultrasonic stimulation onsets and ceases, as is made evident by the vertical black bars. (Note the x- and y-axis scale differences between these plots.) Also evident in A is the immediate rise in V1 amplitude after the ultrasound burst of pulses is complete which signifies that yes, indeed, the brain is activated immediately by ultrasound application in addition to the follow-on activation of the slow waves. B paints a different story, however: The ultrasonic burst evokes a rise in brain activity for the duration of the burst but once the ultrasonic burst is complete the activity amplitude of the brain falls back towards its background state before slow waves become apparent. This suggests that an ultrasonic burst can evoke a rise in brain activation that will carry on to greater amplitude after the burst is complete, and this also suggests that if an ultrasonic burst is held long enough that it can evoke the brain activation to rise to such a level that it will not continue to rise after the burst ceases. Clearly, the ultrasonic pulse count must be chosen wisely to fit the type of brain stimulation desired for a particular experiment or application.

The intensities of different ultrasonic protocols and their associated normalized energy differentials are shown below. To calculate the normalized energy differential of the spike in comparison to the background, the background energy was subtracted from the energy of the spike, and the resulting differences divided by the background energy. Calculation of the normalized energy differential of the residual activity in comparison to the background was calculated in the same way. (In all cases, energy was normalized by the length of time allotted to collect the energy.) The time range of the spike energy, being 0.0-0.2 seconds following stimulation onset, was chosen due to the observation that the spike tends to reside within these bounds. The time range of the background energy, being 0.2-3.8 seconds prior to stimulation onset, was chosen to avoid influence of event segment edge effects (event segments were designated as 4.5 seconds on either side of the onset) and influence of the spike which may appear to have affects before the onset due to filtering. The time range of the residual energy, being 0.2-3.0 seconds following stimulation onset, was chosen to match the range chosen for the CWT plots.

Figure 17 through Figure 20 depict the normalized energies of the spike and the residual for each event according to their I_{spta} values, with results segregated between isoflurane and medetomidine. (N.B., the y-axis and x-axis vary by figure.) This data was generated by mice under either isoflurane or medetomidine and each mouse received one or two ultrasonic intensity levels. Two mice were tested under both isoflurane and medetomidine. It was found in multiple cases that the median was less than zero. These results are juxtaposed with other distributions which have means and medians above zero with statistical significance and occasionally far reaching positive outliers. This suggests that while ultrasonic stimulation can produce neural activation, it can also produce suppression, and when it does generate activation it does not always provide a consistent level of activation. It is possible some intensity levels promote activation, and others promote suppression.

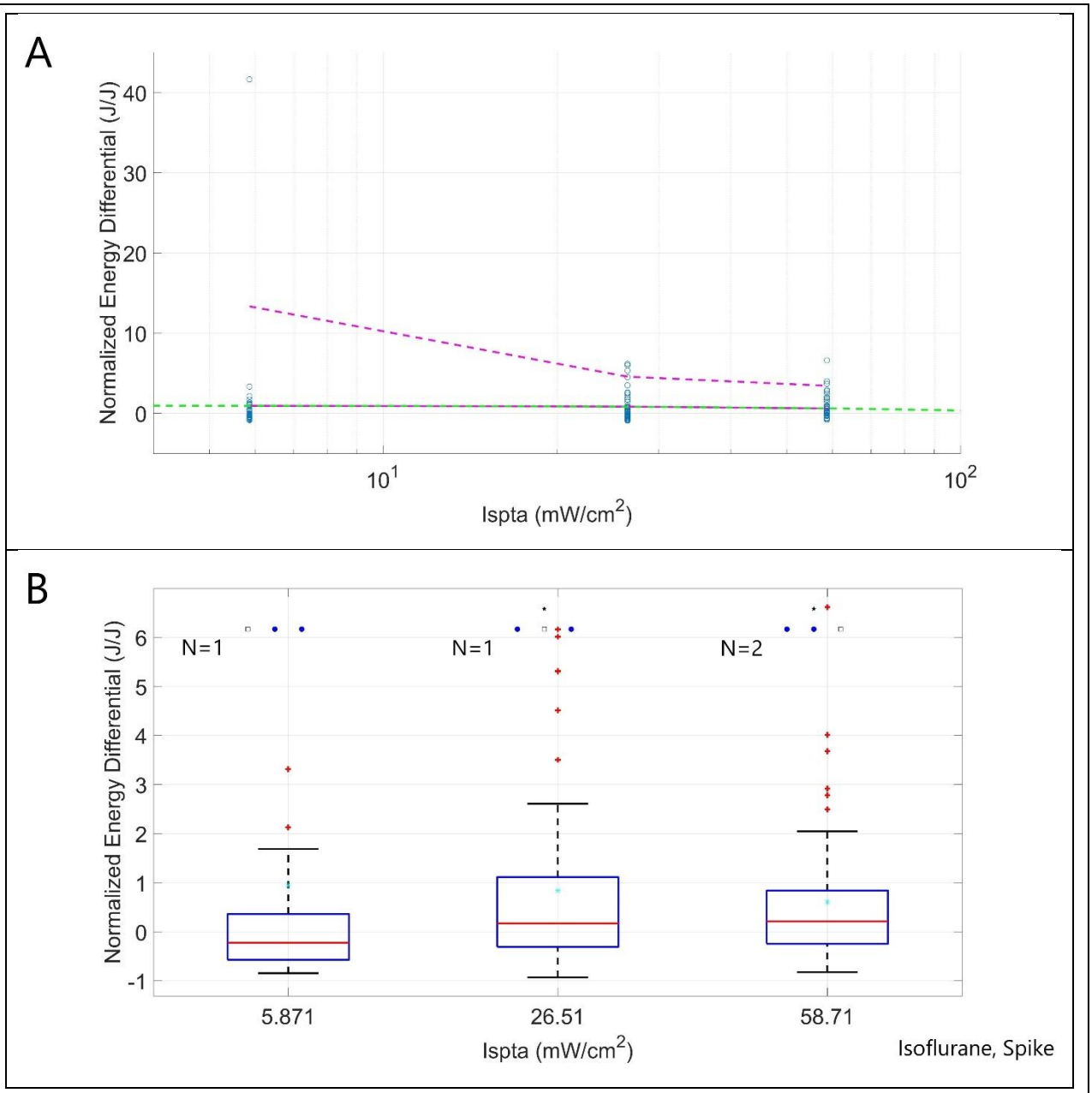

Figure 17: Energy differential of spike at V1 under isoflurane. ECoG results filtered 3-100Hz. (A) All data shown as blue circles. Dashed green best-fit line indicates that its slope is not statistically different from zero. Mean is solid magenta line (here partly obscured by the best-fit line). Dashed magenta line is two standard deviations above the mean. (B) Boxplots show quartiles (notice that one median lies below zero), less outliers which are shown as red plus marks (some of which are beyond the upper limit of the plot window). The number of mice tested is shown. Mean is cyan asterisk. Presence of a black star near the upper edge of the window indicates that the mean is statistically greater than zero per the Wilcoxon signed rank test. The second line of symbols indicate if the mean of the distribution is not statistically different from (blue dot) its respective neighbors per a permutation test with 10000 permutations. Comparison with itself (empty black square) is meaningless apart from orienting the other symbols with their respective distributions. In this case, the permutation test finds all distributions to be not statistically different from each other.

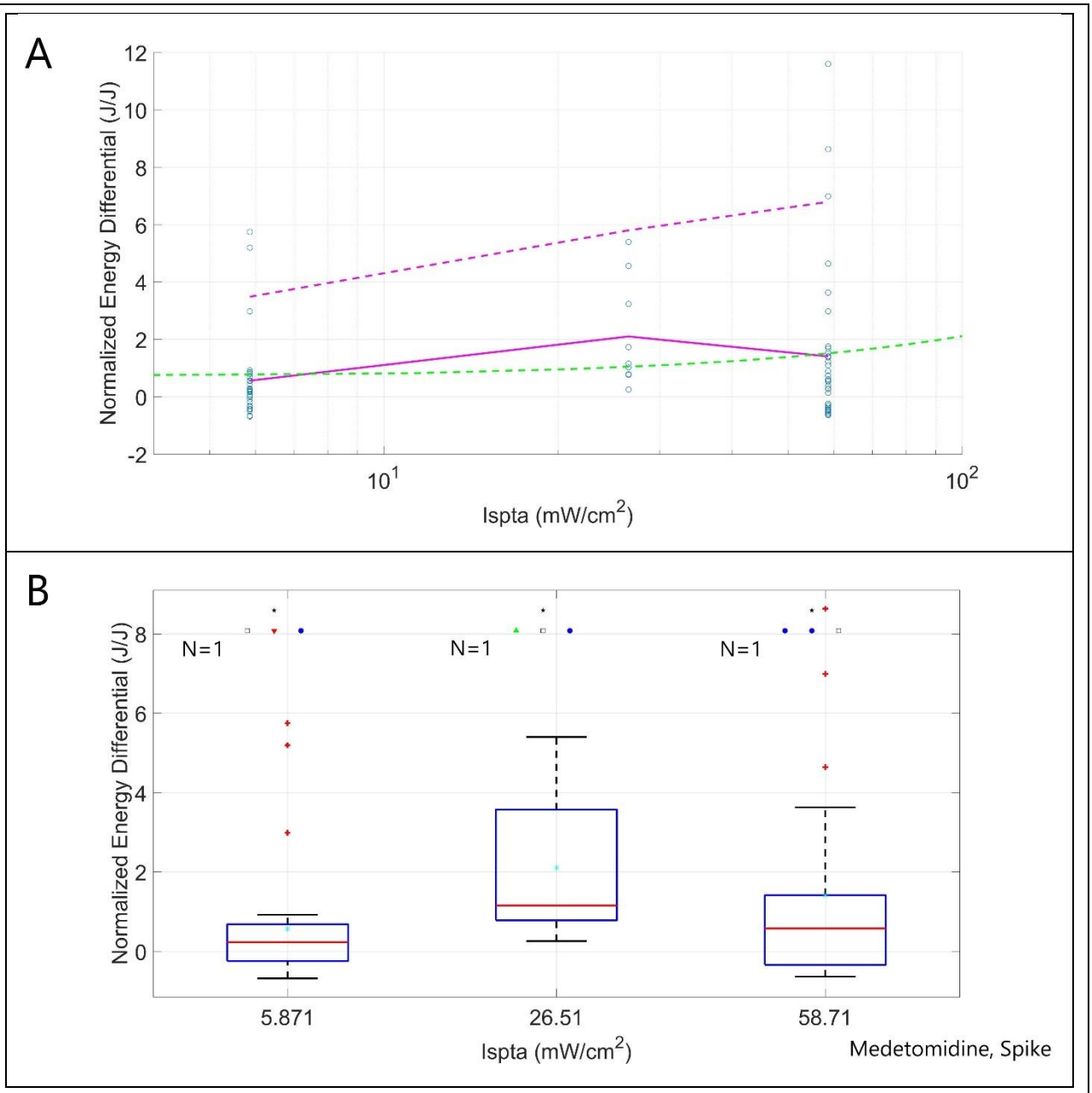

Figure 18: Energy differential of spike at V1 under medetomidine. ECoG results filtered 3-100Hz. (A) All data shown as blue circles. Solid green best-fit line indicates that its slope is statistically different from zero. Mean is solid magenta line. Dashed magenta line is two standard deviations above the mean. (B) Boxplots show quartiles, less outliers which are shown as red plus marks (some of which are beyond the upper limit of the plot window). The number of mice tested is shown. Mean is cyan asterisk. Presence of a black star near the upper edge of the window indicates that the mean is statistically different from zero per the Wilcoxon signed rank test. The second line of symbols indicate if the mean of the distribution is statistically greater than (upward green arrow), statistically less than (downward red arrow), or not statistically different from (blue dot) its respective neighbors per a permutation test with 10000 permutations. Comparison with itself (empty black square) is meaningless apart from orienting the other symbols with their respective distributions.

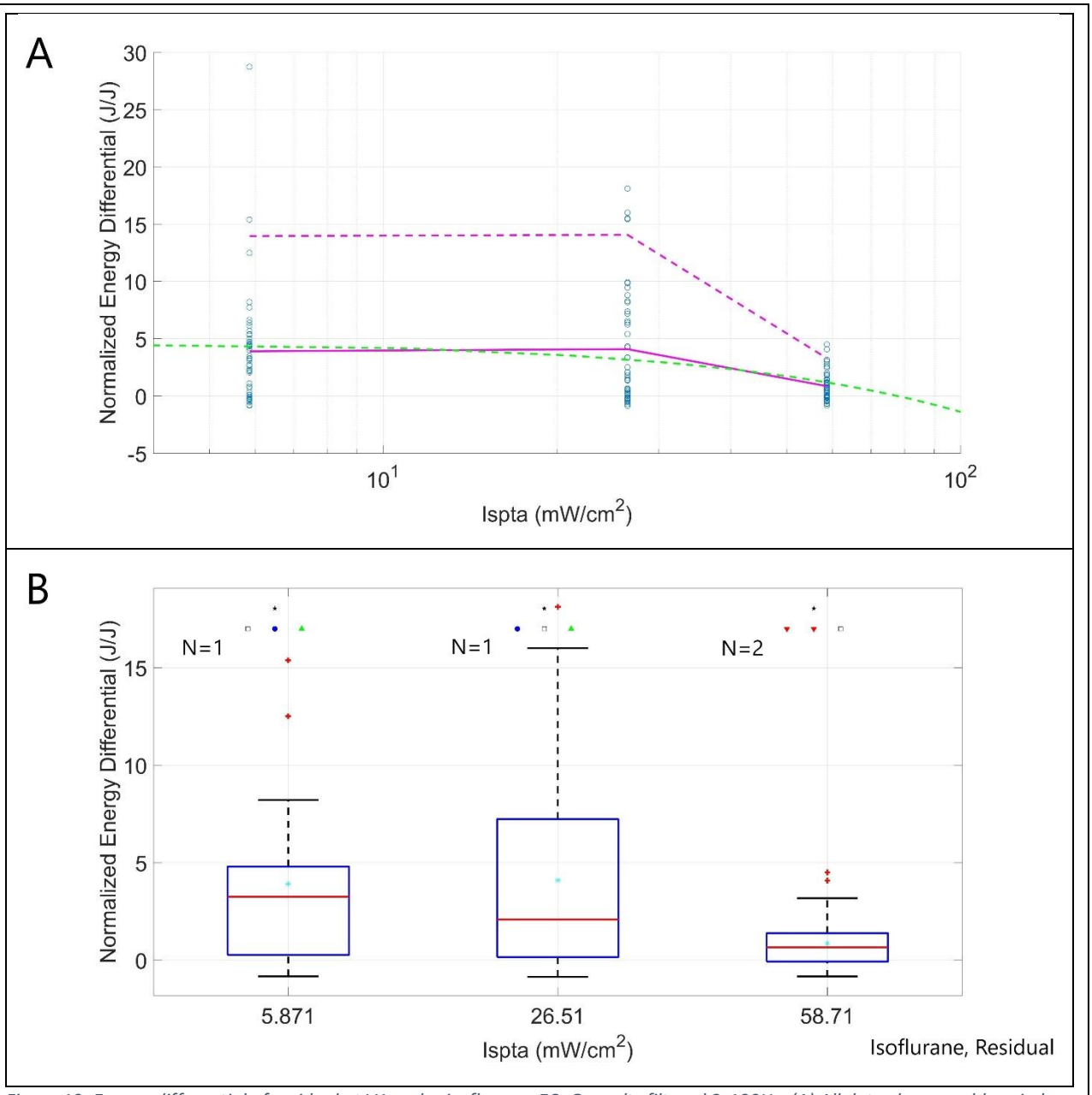

Figure 19: Energy differential of residual at V1 under isoflurane. ECoG results filtered 3-100Hz. (A) All data shown as blue circles. Dashed green best-fit line indicates that its slope is not statistically different from zero. Mean is solid magenta line. Dashed magenta line is two standard deviations above the mean. (B) Boxplots show quartiles, less outliers which are shown as red plus marks (some of which are beyond the upper limit of the plot window). The number of mice tested is shown. Mean is cyan asterisk. Presence of a black star near the upper edge of the window indicates that the mean is statistically different greater than zero per the Wilcoxon signed rank test. The second line of symbols indicate if the mean of the distribution is statistically greater than (upward green arrow), statistically less than (downward red arrow), or not statistically different from (blue dot) its respective neighbors per a permutation test with 10000 permutations. Comparison with itself (empty black square) is meaningless apart from orienting the other symbols with their respective distributions. The distributions with lesser intensities have means statistically higher than the distribution with the strongest intensity in this case. This may indicate that lower intensities increase the slow wave response of the brain when it is under anesthesia. However, the small sample size makes all findings tentative and more studies are needed.

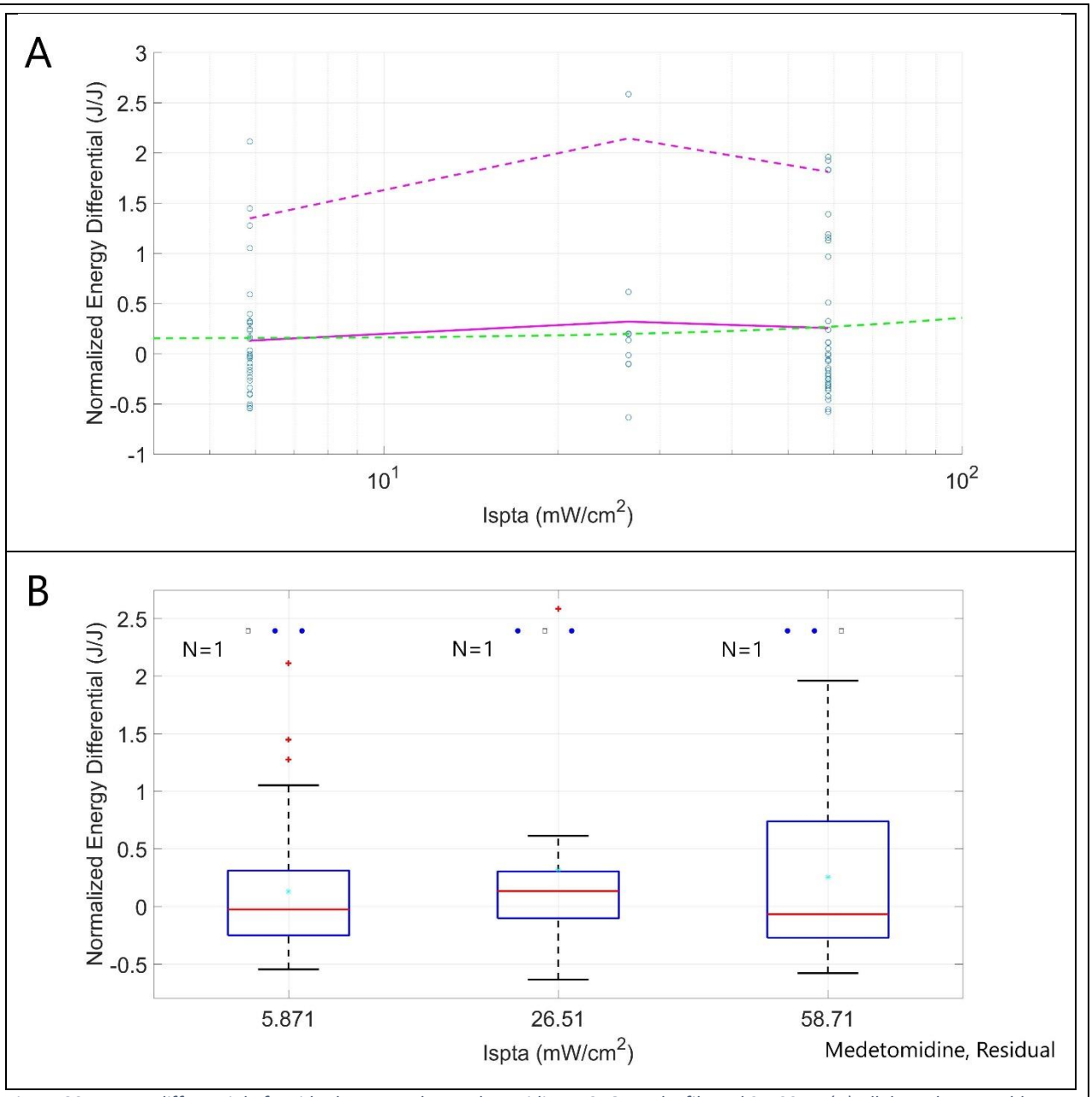

Figure 20: Energy differential of residual at V1 under medetomidine. ECoG results filtered 3-100Hz. (A) All data shown as blue circles. Dashed green best-fit line indicates that its slope is not statistically different from zero. Mean is solid magenta line. Dashed magenta line is two standard deviations above the mean. (B) Boxplots show quartiles, less outliers which are shown as red plus marks. Note that the median lies below zero for two of the distributions. The number of mice tested is shown. Mean is cyan asterisk. Presence of a black star near the upper edge of the window indicates that the mean is statistically different from zero per the Wilcoxon signed rank test. The second line of symbols indicate if the mean of the distribution is not statistically different from (blue dot) its respective neighbors per a permutation test with 10000 permutations. Comparison with itself (empty black square) is meaningless apart from orienting the other symbols with their respective distributions.

None of the cases show a best-fit trend line with a statistically significant linear slope in normalized energy with respect to I_{spta} at a 95% confidence level, 2-sided test, utilizing MATLAB's *fit* and *confint* functions. With these results in mind, it was determined that CWT analysis would be a reasonable approach with respect to number of pulses applied, averaged across different intensity levels.

In the case of the initial spike, the means of different intensities under isoflurane (Figure 17) were not statistically different from one another and under medetomidine (Figure 18) only one intensity differed in the mean from the other two. Except in the case of the lowest intensity under isoflurane, all of the intensities produced means statistically higher than zero across both isoflurane and medetomidine. When the results under medetomidine and isoflurane are compared, the results are within the same order of magnitude. These findings suggest that anesthetized and sedated brain states produce similar spike responses when V1 is stimulated ultrasonically, and that those similarities are fairly robust across different ultrasonic intensities.

In the residual case (being the response following the initial spike as depicted in Figure 4) under isoflurane, all three intensity levels after the initial spike show mean values statistically higher than zero (Figure 19), indicating a presence of slow waves, and in the corresponding residual case under medetomidine none of the intensity levels show mean values statistically higher than zero (Figure 20), indicating an absence of slow waves. This matches the visual stimulation observations and is a pertinent, albeit preliminary, conclusion unto itself signifying that light stimulation of the eye and direct ultrasonic stimulation of V1 produce similar results. Depending on the applications being researched, ultrasonic and visual stimulation techniques may become interchangeable modes of V1 activation.

The differences in amplitude response from isoflurane to medetomidine are considerable, roughly an order of magnitude for some intensities, yet they fail to detract from the finding expressed above. Rather, the differences in amplitude of responses serve to stoke further exploration of the effects of varying intensities. Although no statistically significant trends were found in these data, extrapolation should not be trusted at great lengths and neural responses to ultrasonic stimulation intensity may be non-linear; i.e., more research is needed to determine if higher intensities of ultrasound will produce neural responses in the sedated brain (medetomidine) to the same order of magnitude as the neural responses in the brain under anesthesia (isoflurane), in addition to determining the extent of the robustness of the current findings.

CWT analysis of the signals was performed in the same way as with the visual stimulation of healthy mice. Modifying the wavelet to favor time resolution was considered but ultimately decided against in order to reduce the variable count when comparing visual and ultrasonic stimulation. CWT results are shown from V1, S1, and A1 in Figure 21 for mice under isoflurane anesthesia when 10 pulses of ultrasound stimulation were applied to V1. In comparison to the isoflurane results under visual stimulation, the slow waves are evident. In contrast, the spike is not. This data may suggest that certain ultrasonic stimulation protocols of V1, here a very short ultrasound protocol with only 10 pulses under isoflurane may be able to bypass the neural processes which cause a strong spike yet still trigger the neural processes which cause slow waves to occur. It is hypothesized that this is not wholly

unreasonable because signals generated at the retina of the eye (in response to visual stimulation) must traverse through the lateral geniculate nucleus (LGN) before the visual cortex may be activated (Tang J 2016, Kerschensteiner D 2017), and thus the light stimulation has the opportunity to activate different processes than direct ultrasonic stimulation of V1 would. This is, of course, a hypothesis only. Other details worth noting are the apparent persistence of the slow waves over time and the curiously weak activity in the low 20 Hz range. Whether these attributes are associated with the lack of a spike is unclear. Concerning the slow wave duration, this ultrasonically stimulated case appears to have a stronger duration than that of visual stimulation, which may point to not yet fully described neural activation process differences between visual and ultrasonic stimulation.

An interesting contrast arises when we used 100 pulses of ultrasound rather than 10 pulses as above, shown in Figure 22. These results resemble the visual stimulation under isoflurane results in that a spike is apparent in V1, yet the spike is less intense than the following slow waves. These data may suggest that, at least for this longer ultrasonic protocol, while 10 pulses of ultrasound may not evoke a strong initial pulse, 100 pulses of ultrasound can, and that specifically in the brain region to which ultrasound is applied. Noting that the spike in the 100 pulses cases peaks quite close to *t=0* suggests that 10 pulses may be slightly too few to evoke the statistically significant spike at the onset of the ultrasonic application. Since it has been shown that V1 provides feedback to the LGN in at least some mammals (Fitzpatrick D 1994, Briggs F 2007), it is reasonable to hypothesize that different protocols of direct ultrasonic stimulation to V1 may provide different feedback to the LGN, and thus different signals recorded by ECoG. Concerning the slow wave duration, this ultrasonically stimulated case appears to have a weaker duration than that of visual stimulation or its previously described 100 pulse protocol counterparts. In addition to the question of basic ultrasonic and visual neural activation processes, questions arise whether a brief burst of ultrasound (e.g., 10 pulses) can reliably generate longer lasting slow waves than a longer burst of ultrasound (e.g., 100 pulses).

Results of ultrasonic stimulation under sedative medetomidine are shown in Figure 23 with 10 pulses of ultrasonic stimulation. A spike is present in V1 but not in A1 or S1 and slow waves are very weak or non-existent in all brain regions. Both of these findings are reminiscent of visual stimulation under medetomidine as shown in Figure 14. This implies that the techniques of ultrasonic stimulation of V1 and of visual stimulation under medetomidine produce comparable results. Despite the non-statistically significant trend for spike energy under medetomidine with respect to intensity as show in Figure 18, it is still tempting to suggest that differing levels of activation between visual and ultrasonic stimulation (i.e., intensity of light to the retina and intensity of ultrasound to V1) are enough to explain away the difference in magnitude of neural activation. The levels of statistical significance under medetomidine in the results of light and ultrasonic stimulation are admittedly different, but as argued previously concerning the differences in magnitude of the responses between the anesthetized and sedated brain states, there is opportunity for different levels of ultrasonic intensities to reduce the differences in magnitude between the responses due to ultrasonic and light stimulation. Ultrasonic intensities beyond the relatively narrow range considered in this thesis may have greater effects: After all, extrapolation should be cautioned, especially in this case of a small sample sizes.

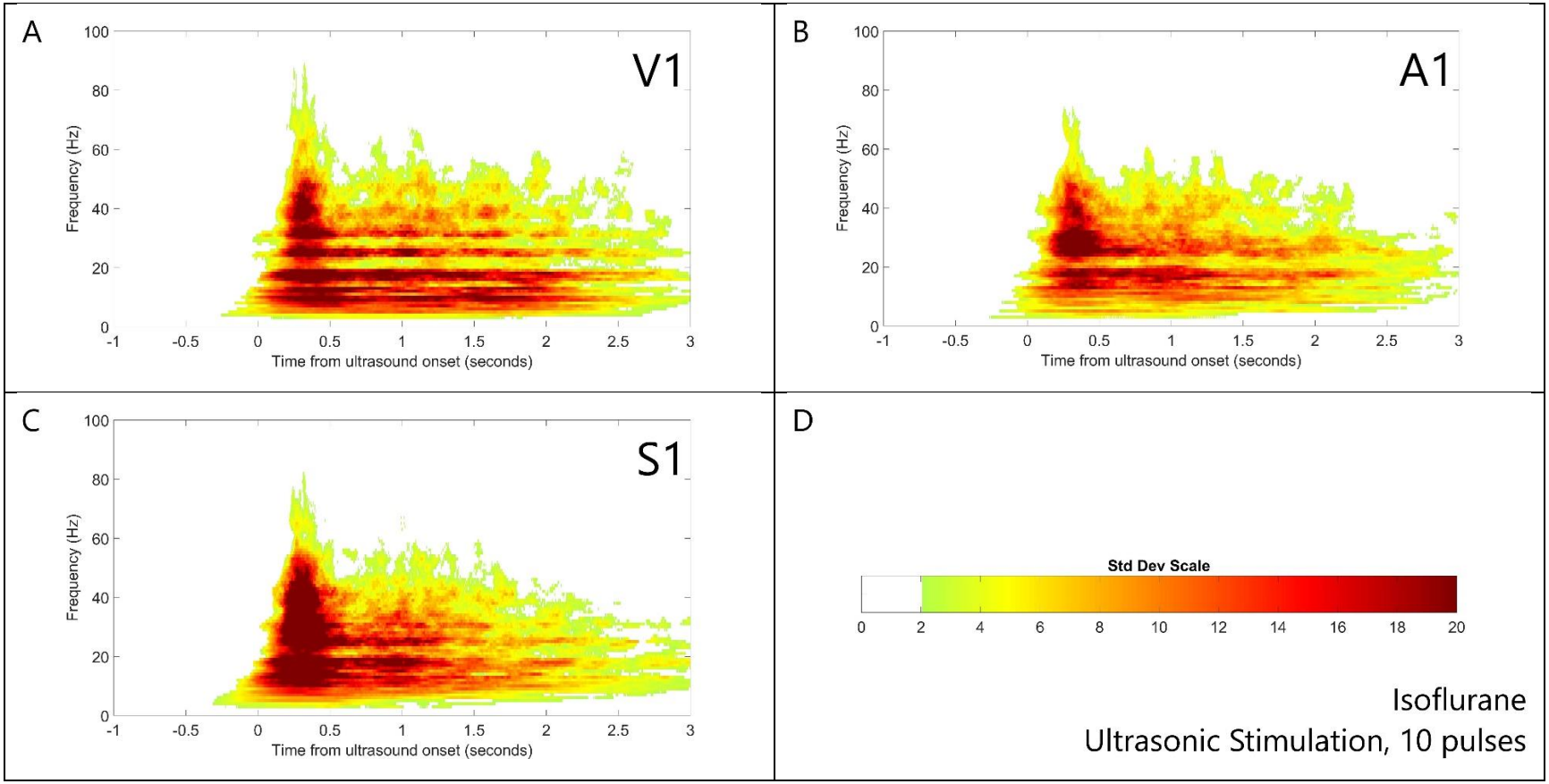

Figure 21: CWT recordings of ECoG, bandwidth frequency 3.0 Hz, standard deviation mask at 2, with global cluster analysis of 3 mice under isoflurane ultrasonically stimulated for 10 pulses at 1050 Hz with I_{spta} 5.87-26.5 mW/cm^2. (A) V1 response exhibits no apparent spike but strong slow wave activity. (B) A1 response exhibits no apparent spike but strong slow wave activity. (C) S1 response exhibits no apparent spike but strong slow wave activity. Onset of slow wave appears stronger than the other brain regions, although the slow waves appear to taper off into the masked region at roughly the same rate which may suggest a non-linear relationship between the strength of the slow wave onset and slow wave duration. (D) Standard deviations from the mean power of the signal prior to stimulation onset.

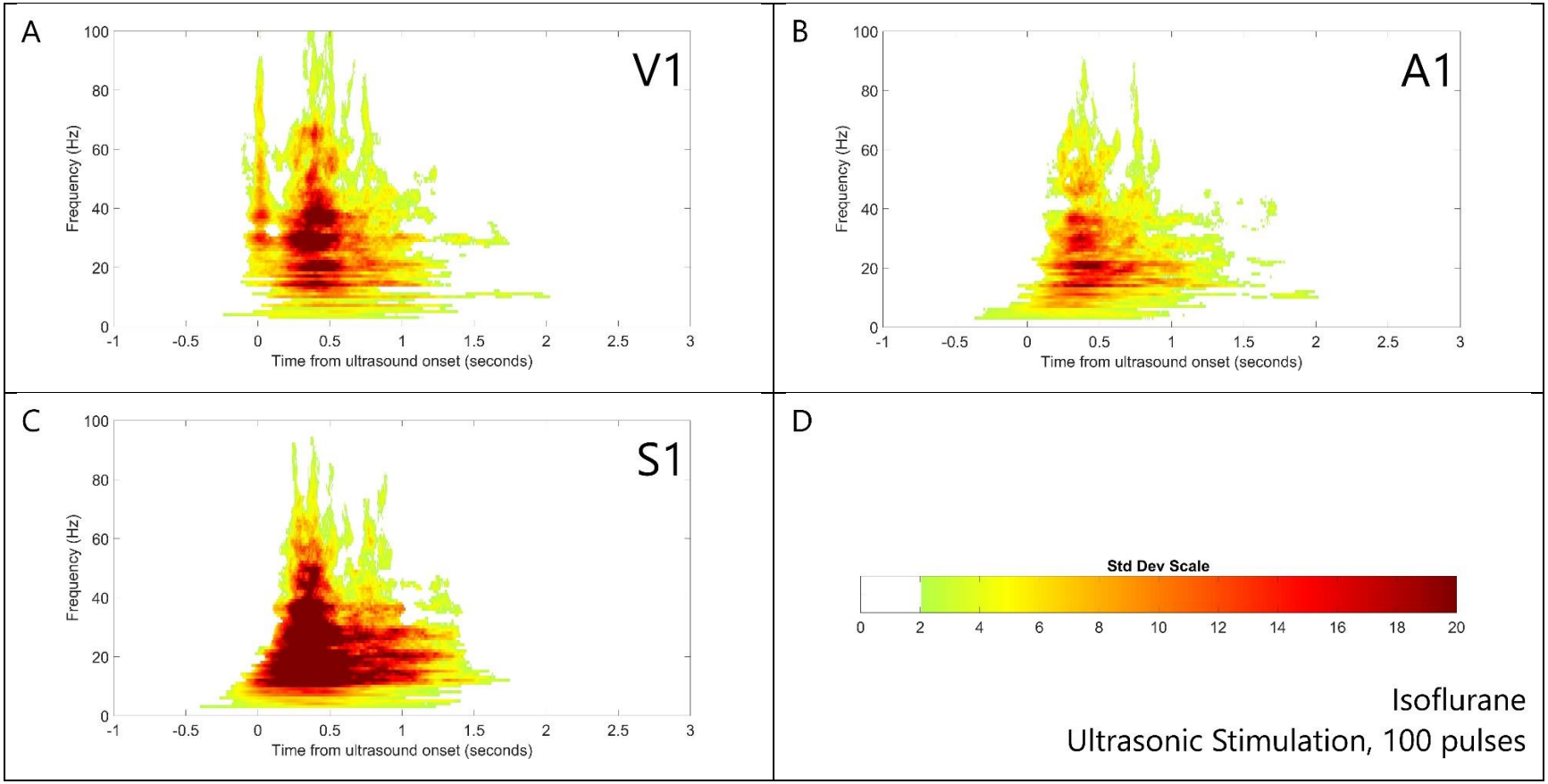

Figure 22: CWT recordings of ECoG, bandwidth frequency 3.0 Hz, standard deviation mask at 2, with global cluster analysis of 2 mice under isoflurane ultrasonically stimulated for 100 pulses at 1050 Hz with I_{spta} 58.7-739 mW/cm^2. (A) V1 response exhibits moderate spike and a moderate slow wave activity. (B) A1 response exhibits weak spike and moderate wave activity. (C) S1 response exhibits weak spike and moderate activity. Onset of slow wave appears stronger than the other brain regions, although the slow waves appear to taper off into the masked region at roughly the same rate which may suggest a non-linear relationship between the strength of the slow wave onset and slow wave duration. (D) Standard deviations from the mean power of the signal prior to stimulation onset.

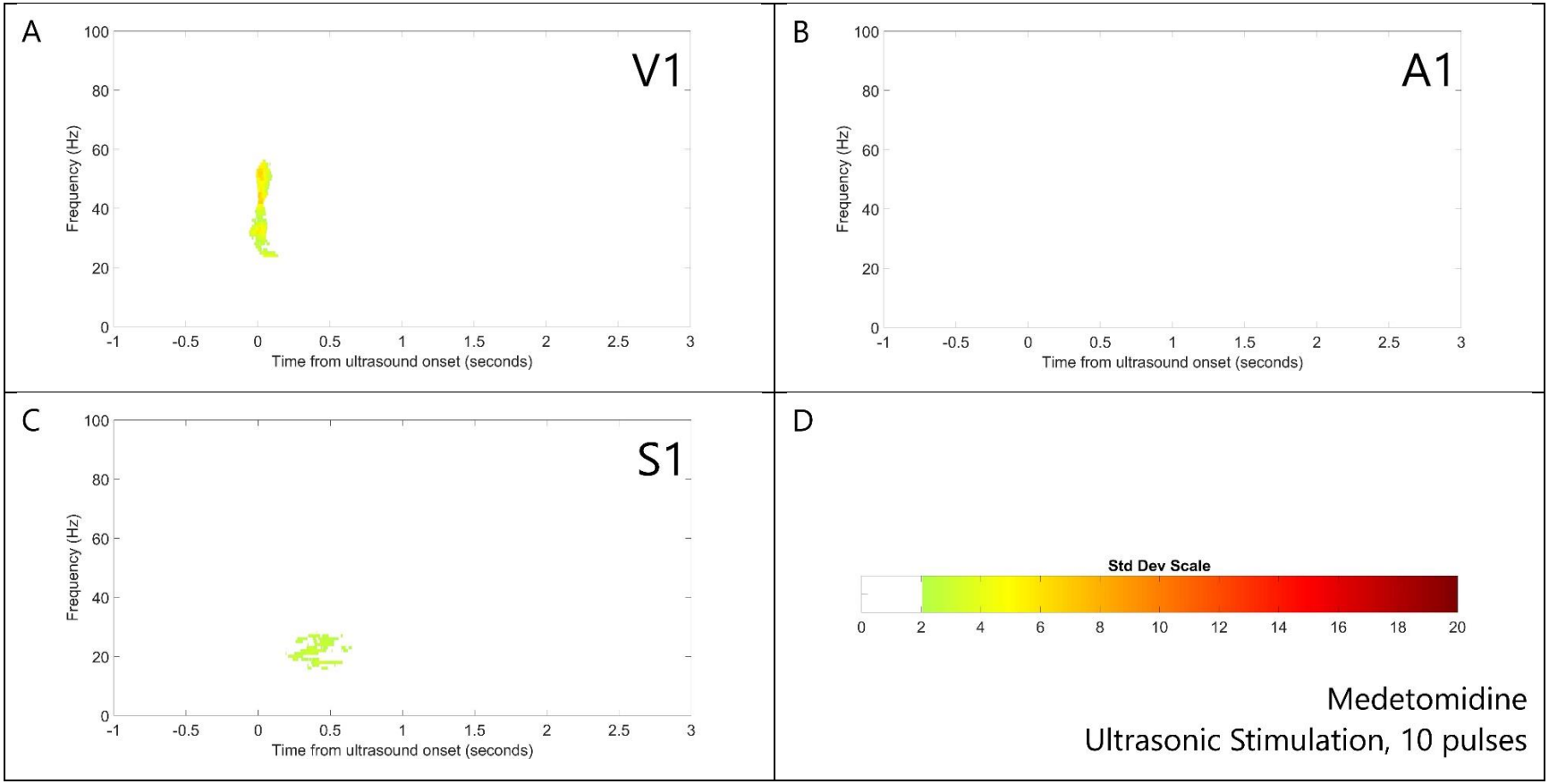

Figure 23: CWT recordings of ECoG, bandwidth frequency 3.0 Hz, standard deviation mask at 2, with global cluster analysis of 1 mouse under medetomidine ultrasonically stimulated for 10 pulses at 1050 Hz with I_{spta} 5.87-26.5 mW/cm^2. (A) V1 response exhibits a weak spike and no slow wave activity. (B) A1 response exhibits no statistically significant results whatsoever. (C) S1 response exhibits no spike and weak slow wave activity. (D) Standard deviations from the mean power of the signal prior to stimulation onset.

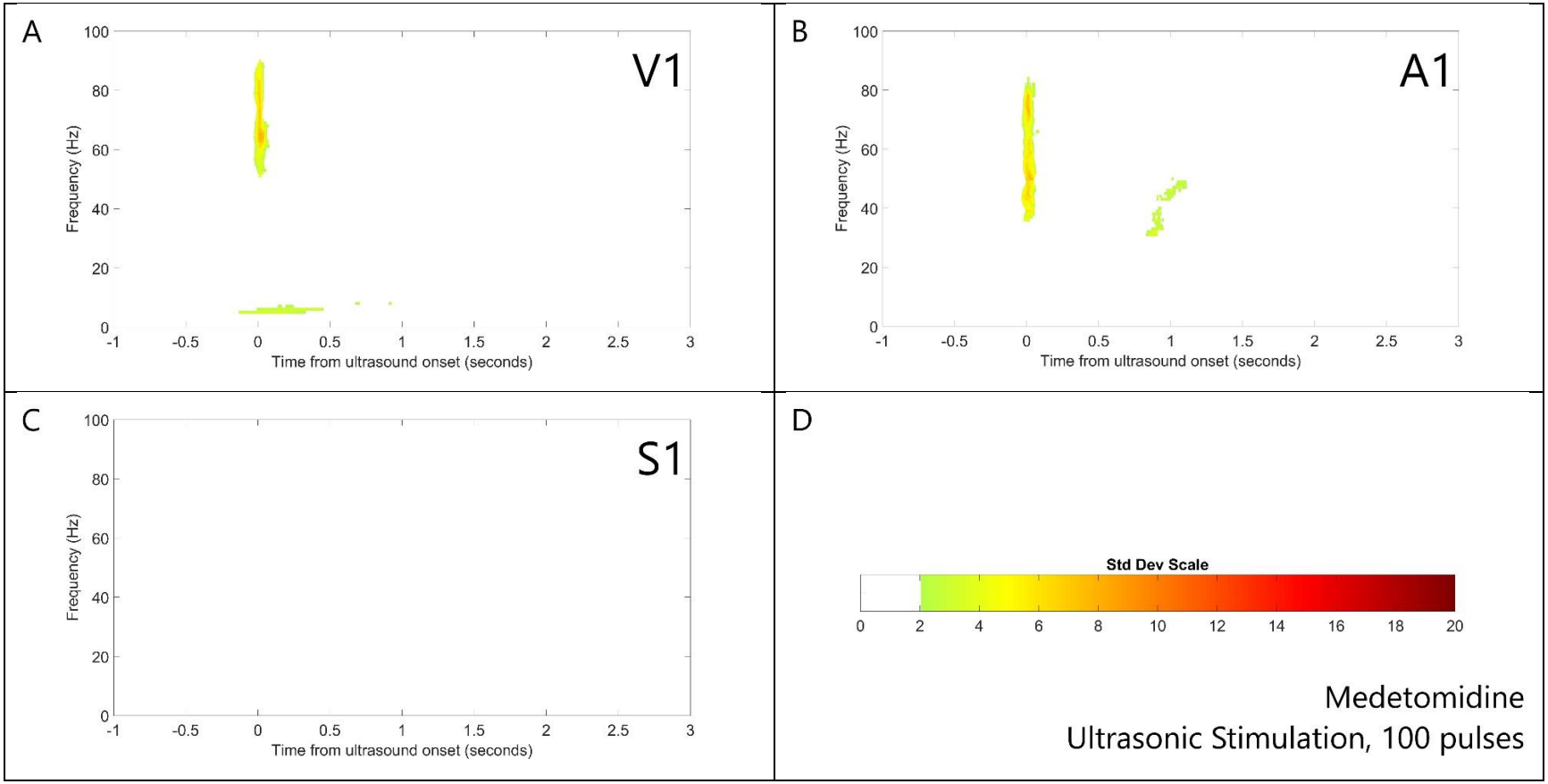

Figure 24: CWT recordings of ECoG, bandwidth frequency 3.0 Hz, standard deviation mask at 2, with global cluster analysis of 2 mice under medetomidine ultrasonically stimulated for 100 pulses at 1050 Hz with I_{spta} 58.7-147 mW/cm^2. (A) V1 response exhibits a weak spike and no slow wave activity. (B) A1 response exhibits a weak spike and weak slow wave activity. (C) S1 response exhibits no statistically significant results whatsoever. (D) Standard deviations from the mean power of the signal prior to stimulation onset.

Results of ultrasonic stimulation under sedative medetomidine are shown in Figure 24 with 100 pulses of ultrasonic stimulation. The most immediate difference between their 10 pulse counterparts is the existence of an unmasked spike response in A1 which suggests that, perhaps, more than 10 pulses are required to reliably evoke an immediate response when the brain is under medetomidine. Of course, this result is likely influenced by bleed from V1, especially when the proximity of A1 and V1 is considered. A1 aside, the V1 and S1 results are similar to the 10 pulse results displayed in Figure 23 in that the slow waves are not visible. V1 and S1 are also similar in the existence or lack of existence of a spike. On the whole, this ultrasonic stimulation protocol under medetomidine produces a similar appearance to visual stimulation under medetomidine as shown in Figure 14. This drives the preliminary conclusions that, firstly, direct ultrasonic stimulation of V1 and indirect stimulation of V1 via light cast on the retina create comparable effects with regards to the presence or absence of slow waves under different brain states and that, secondly, hypotheses of the differences between these stimulation techniques, specifically in regards to the generation of an initial spike, provide grounds for further investigation.

DISCUSSION

Regarding visual stimulation, the strength of the response in V1 as compared to A1 and S1 confirms that the visual stimulations are successful and provides a control for studies involving ultrasonic activation. The mean energy for both the spike and the residual and for both isoflurane and medetomidine increased with respect to background neural activity, signifying successful activation and indicating calcium (Ca^{2+}) slow waves in the case of isoflurane. In contrast to medetomidine, the medetomidine residual, although statistically greater than zero, is weak in comparison with the isoflurane residual and is not representative of slow waves, as is depicted in the CWT analysis. The primary result is the observed presence and absence of slow waves when the brain is under isoflurane and medetomidine, respectively, and is consistent with the general understanding of slow waves.

Ultrasonic stimulation provides both similarities and contrasts to visual stimulation. It was shown in A that the brain is activated immediately by ultrasound application in addition to the follow-on activation of the slow waves by the immediate rise in V1 amplitude after the cessation of the ultrasonic burst. In contrast, B showed that a longer ultrasonic burst evokes a rise in brain activity for the duration of the burst alone before slow waves become apparent, suggesting that ultrasonic bursts of differing lengths may produce different results. In this particular case it is seen that a short ultrasonic burst can evoke a rise in brain activation that will carry on to greater amplitude after the burst is complete, and a longer ultrasonic burst can evoke brain activation which will not be followed by a rise in activity after the cessation of the burst. An additional finding is that while ultrasonic stimulation can produce neural activation, it does not always do so, and when it does so it does not always provide a consistent level of activation. Fortunately, the same may be said about visual stimulation as seen in Figure 12 which suggests that visually stimulated events and ultrasonically stimulated events have similar attributes despite their distinct differences in magnitude of evoked response as seen with the specific ultrasonic protocols used in this research.

In addition to timeseries analysis, CWT analysis and energy analysis across multiple intensity levels show that ultrasonic stimulation of V1 under isoflurane anesthesia is marked by slow waves and under medetomidine sedative is marked by an absence of slow waves. This matches the visual stimulation observations and is an important preliminary conclusion: Indirect light stimulation of the eye and direct ultrasonic stimulation of V1 produce similar ECoG-recordable results. The differences in the presence or absence of the initial spike under different combinations of ultrasonic protocols and brain states may point to inter-regional processes within the brain, specifically between V1 and LGN, which are not yet well understood when V1 is directly activated by ultrasound. Because stimulation-evoked initial spikes and slow waves are relatively distinct as shown in the CWT analysis, it is reasonable to consider both of these observations as separate findings. All conclusions are tentative pending future trials with more mice.

REMAINING OPEN QUESTIONS

Questions remain. Regarding the study of the healthy mice, the origins of any noise on the results is, although hypothesized, still unclear as is the magnitude of the effects of the noises. As with any preliminary research on small sample sizes, it remains to be seen how the described responses under different parameters hold up when data is taken across a larger sample of mice. The difference in neural responses between visual stimulation and direct ultrasonic stimulation of V1, if it holds up after more studies, raises questions of the detailed interworking of the brain.

In regards to this study specifically, more data is desired to strengthen confidence in the results with more experimentation regarding the utilized variables of intensity and number of pulses, and in regards to variables which were held fixed such as the carrier frequency of 2.00 MHz and the pulse repetition frequency of 1050 Hz. As is agreed upon throughout the literature, different ultrasonic protocols often have different effects on neural tissue, which make these many variables important to consider. This research may be aided by a better understanding of the precise mechanism by which ultrasound stimulates neurons. Results generated with more extensive variation in intensity are perhaps the most immediately viable, and these results will be important to consider in order to determine if ultrasonic stimulation of V1 can produce results to the same level of magnitude as that of light stimulation of the retina. Research of the relationships between V1 and other regions of the brain, particularly LGN, are of also interest to determine how direct ultrasonic activation of V1 and indirect activation of V1 via light cast on the retina compare. Such studies may be more difficult to perform and the differences between the results may be more nuanced.

While stimulation of V1 was the specific focus of this thesis, a host of opportunity remains to research the comparisons between direct ultrasonic stimulation and indirect sensory-driven stimulation of different brain areas, such as S1 and A1. Such research would reveal if the similarities and differences between the effects of stimulation modalities under different brain states are specific to discrete regions of the cortex or are general throughout the cortex. These results would likely be obtainable with roughly the same level of effort and expertise required for the experiments represented by this thesis because the ultrasonic transducer would simply need to be repositioned and the light stimulation could be

swapped for other simple simulation techniques such as pinching for stimulation of S1 and speakers for stimulation of A1.

CONCLUSION

Concerning the study of healthy mice, isoflurane and medetomidine cause different responses in the brain when visual stimulation is applied, specifically regarding the presence and strength of, or absence of, slow waves. Ultrasonic stimulation of V1 causes similar responses and thus may be employed to directly stimulate activity with or without slow waves as desired. This result is true when averaged across multiple I_{spta} levels and many individual ultrasonic stimulation events as shown in the CWT figures. The presence or absence of the initial spike as evoked by ultrasonic stimulation leaves more to explore but provides a tentative conclusion that differing ultrasonic protocols trigger different neural processes, or at least different levels of expression of those processes. Due to the small sample size, more research is needed to validate these promising results which may pave the way toward a more thorough understanding of the effects of ultrasonic stimulation of different brain states.

ACKNOWLEDGEMENTS

I would like to thank Curtis Easton for his guidance from a neuroscience perspective and I would like to thank him and the rest of Mourad group for their efforts in the lab generating the data analyzed here. My gratitude also extends to my Committee Members: Dr. Ghirmai, Dr. Cao, and Dr. Mourad, the latter of whom deserves special thanks for working with me through the entire thesis process. Finally, I would like to thank The Boeing Company for funding much of my MSEE experience and my managers who have supported me along the way.

REFERENCES

Bauer R, Martin E, Haegele-Link S, Kaegi G, von Specht M, Werner B. 2014. "Parkinsonism & Related Disorders." *Noninvasive functional neurosurgery using transcranial MR imaging-guided focused ultrasound* Volume 20, S197 - S199.

Bellesi M, Riedner BA, Garcia-Molina GN, Cirelli C, Tononi G. 2014. "Enhancement of sleep slow waves: underlying mechanisms and practical consequences." *Frontiers in Systems Neuroscience* 8, 208.

Bennett CM, Baird AA, Miller MB, Wolford GL. 2011. "Neural Correlates of Interspecies Perspective Taking in the Post-Mortem Atlantic Salmon: An Argument For Proper Multiple Comparisons Correction." *Journal of Serendipitous and Unexpected Results* Vol. 1, pp. 1-5.

Briggs F, Usrey WM. 2007. "A Fast, Reciprocal Pathway between the Lateral Geniculate Nucleus and Visual Cortex in the Macaque Monkey." *The Journal of Neuroscienc : The Official Journal of the Society for Neuroscience* 27(20), 5431–5436.

Bystritsky A, Korb AS, Douglas PK, Cohen MS, Melega WP, Mulgaonkar AP, DeSalles A, Min BK, Yoo SS. 2011. "A review of low-intensity focused ultrasound pulsation." *Brain Stimulation: Basic, Translational, and Clinical Research in Neuromodulation* Volume 4, Issue 3, 125 - 136.

Darvas F, Mehić E, Caler CJ, Ojemann JG, Mourad PD. 2016. "Toward Deep Brain Monitoring with Superficial EEG Sensors Plus Neuromodulatory Focused Ultrasound." *Ultrasound in Medicine and Biology* Volume 42, Issue 8, 1834 - 1847.

Errico C, Osmanski BF, Pezet S, Couture O, Lenkei Z, Tanter M. 2015. "Transcranial Functional Ultrasound Imaging of the Brain using Microbubble-Enhanced Ultrasensitive Doppler." *NeuroImage* 124.

Fitzpatrick D, Usrey W, Schofield B, Einstein G. 1994. "The sublaminar organization of corticogeniculate neurons in layer 6 of macaque striate cortex." *Visual Neuroscience* 11(2), 307-315.

Funayama K, Minamisawa G, Matsumoto N, Ban H, Chan AW, Matsuki N, Murphy TH, Ikegaya Y. 2015. "Neocortical Rebound Depolarization Enhances Visual Perception." *PLoS Biology* 13(8), e1002231.

Gavrilov LR, et al. 1996. "Application of focused ultrasound for the stimulation of neural structures." *Ultrasound in Medicine and Biology* Volume 22, Issue 2, 179 - 192.

Grossman N, Bono D, Dedic N, Kodandaramaiah SB, Rudenko A, Suk HJ, Cassara AM, Neufeld E, Kuster N, Tsai LH, Pascual-Leone A, Boyden ES. 2017. "Noninvasive Deep Brain Stimulation via Temporally Interfering Electric Fields." *Cell* Volume 169, Issue 6, 1029 - 1041.e16.

Kerschensteiner D, Guido W. 2017. "Organization of the dorsal lateral geniculate nucleus in the mouse." *Visual Neuroscience* 34, E008.

Lin WT, Chen RC, Lu WW, Liu SH, Yang FY. 2015. "Protective effects of low-intensity pulsed ultrasound on aluminum-induced cerebral damage in Alzheimer's disease rat model." *Scientific Reports* 5, 9671.

Lipsman N, Schwartz ML, Huang Y, Lee L, Sankar T, Chapman M, Hynynen K, Lozano AM. 2013. "MR-guided focused ultrasound thalamotomy for essential tremor: a proof-of-concept study." *The Lancet Neurology* Volume 12, Issue 5, 462 - 468.

McClintic AM, King BH, Webb SJ, Mourad PD. 2014. "Mice exposed to diagnostic ultrasound in utero are less social and more active in social situations relative to controls." *Autism Research : Official Journal of the International Society for Autism Research* 7(3), 295–304.

Mehić E, Xu JM, Caler CJ, Coulson NK, Moritz CT, Mourad PD. 2014. "Increased Anatomical Specificity of Neuromodulation via Modulated Focused Ultrasound." *PLoS ONE* 9(2): e86939.

Mesiwala AH, Farrell L, Wenzel HJ, Silbergeld DL, Crum LA, Winn HR, Mourad PD. 2002. "High-intensity focused ultrasound selectively disrupts the blood-brain barrier in vivo." *Ultrasound in Medicine and Biology* Volume 28 , Issue 3 , 389 - 400.

Miller DL. 1991. "Update on safety of diagnostic ultrasonography." *J. Clin. Ultrasound* 19: 531-540.

Minamisawa G, Funayama K, Matsumoto N, Matsuki N, Ikegaya Y,. 2017. "Flashing Lights Induce Prolonged Distortions in Visual Cortical Responses and Visual Perception." *eNeuro* 4(3), ENEURO.0304–16.2017.

Olmstead TA, Chiarelli P, Dewees D, Griggs D, McClintic AM, Myroniv A, Becker K, Goverman JM, Mourad PD. 2018. "Transcranial and pulsed focused ultrasound that activates brain can accelerate remyelination in a mouse model of multiple sclerosis." *Unpublished manuscript, University of Washington, Seattle, WA.*

Plaksin M, Shoham S, Kimmel E. 2014. "Intramembrane Cavitation as a Predictive Bio-Piezoelectric Mechanism for Ultrasonic Brain Stimulation." *Phys. Rev. X* Volume 4, Issue 1, 011004.

Rezayat E, Toostani IG. 2016. "A Review on Brain Stimulation Using Low Intensity Focused Ultrasound." *Basic and Clinical Neuroscience* 7(3), 187–194.

Schmid F, Wachsmuth L, Schwalm M, Prouvot PH, Jubal ER, Fois C, Pramanik G, Zimmer C, Faber C, Stroh A. 2015. "Assessing sensory versus optogenetic network activation by combining (o)fMRI with optical Ca2+ recordings." *Journal of Cerebral Blood Flow & Metabolism* Vol 36, Issue 11, pp. 1885 - 1900.

Schwalm M, Schmid F, Wachsmuth L, Backhaus H, Kronfeld A, Aedo Jury F, Prouvot PH, Fois C, Albers F, van Alst T, Faber C, Stroh A. 2017. "Cortex-wide BOLD fMRI activity reflects locally-recorded slow oscillation-associated calcium waves." *eLife* Vol. 6.

Seo D, Neely RM, Shen K, Singhal U, Alon E, Rabaey JM, Carmena JM, Maharbiz MM. 2016. "Wireless Recording in the Peripheral Nervous System with Ultrasonic Neural Dust." *Neuron* Volume 91, Issue 3, 529 - 539.

Stroh A, Adelsberger H, Groh A, Rühlmann C, Fischer S, Schierloh A, Deisseroth K, Konnerth A. 2013. "Making Waves: Initiation and Propagation of Corticothalamic Ca2+ Waves In Vivo." *Neuron* Volume 77, Issue 6, 1136 - 1150.

Sugita Yoichi, et al. 2008. "Nitric Oxide Generation Directly Responds to Ultrasound Exposure." *Ultrasound in Medicine and Biology* Volume 34, Issue 3, 487 - 493.

Tang J, Ardila Jimenez SC, Chakraborty S, Schultz SR. 2016. "Visual Receptive Field Properties of Neurons in the Mouse Lateral Geniculate Nucleus." *PLoS ONE* 11(1), e0146017.

Tufail Y, Matyushov A, Baldwin N, Tauchmann ML, Georges J, Yoshihiro A, Tillery SIH, Tyler WJ. 2010. "Transcranial Pulsed Ultrasound Stimulates Intact Brain Circuits." *Neuron* 66(5), 681–694.

Tyler WJ, Tufail Y, Finsterwald M, Tauchmann ML, Olson EJ, Majestic C. 2008. "Remote Excitation of Neuronal Circuits Using Low-Intensity, Low-Frequency Ultrasound." *PLoS ONE* 3(10), e3511.

Webb SJ, Garrison MM, Bernier R, McClintic AM, King BH, Mourad PD. 2017. "Severity of ASD symptoms and their correlation with the presence of copy number variations and exposure to first trimester ultrasound." *Autism Research* 10: 472-484.

Yoo SS, Bystritsky A, Lee JH, Zhang Y, Fischer K, Min BK, McDannold NJ, Pascual-Leone A, Jolesz FA. 2011. "Focused ultrasound modulates region-specific brain activity." *Neuroimage* 56(3), 1267–1275.